MOBILE SPEED ESTIMATION FOR

HIERARCHICAL WIRELESS NETWORK

A Thesis presented to the Faculty of the Graduate School
University of Missouri - Columbia

In Partial Fulfillment
Of the Requirements for the Degree
Master of Science

---

by
YU NING

Dr. Chengshan Xiao, Thesis Supervisor

JULY 2005

The undersigned, appointed by the Dean of the Graduate School, have examined the thesis entitled.

MOBILE SPEED ESTIMATION FOR

HIERARCHICAL WIRELESS NETWORK

Presented by Yu Ning

A candidate for the degree of Master of Science

And hereby certify that in their opinion it is worthy of acceptance.

Dr. Chengshan Xiao

Dr. Dominic K.C. Ho

Dr. Haibin Lu

ACKNOWLEDGEMENTS

I would like to thank my thesis adviser, Dr. Chengshan Xiao, for introducing me into the world of wireless communication, for guiding me all the way through my master work, and for providing me with supports in both my research and my life.

I'm also grateful to my dissertation committee member, Dr. Dominic Ho and Dr. Haibin Lu, for taking time from their busy schedules serving in my degree committee.

I'm thankful to my current and previous group-mates: Dr. Yahong R. Zheng, Dr. Sang-Yick Leong, Dr. Liang Hong, Dr. Jianfei Cai, Dr. Lei Cao, Mr. Min Wu, Mr. Yunhong Li, Ms. Xiaoning Lu, for their help and their priceless friendship.

Finally, I would like to thank my parents, who raised me with tremendous love and always inspire me when I grew up, and my husband, Jingxian Wu, who provides me great encouragement and support during my master study. Without their help, it's impossible for me to reach this stage.

MOBILE SPEED ESTIMATION FOR HIERARCHICAL WIRELESS NETWORK

Yu Ning

Dr. Chengshan Xiao, Thesis Supervisor

ABSTRACT

The implementation of hierarchical cellular system, which can effectively reduce the number of handoffs thus significantly improve the overall system capacity, requires the knowledge of mobile user speed at the base station. This thesis focuses on the development of a mobile speed estimation algorithm for practical wireless information system. The statistical properties of different wireless propagation environments are analyzed based on their respective mathematical reference models. The analytical results are applied to facilitate the algorithm design. The mobile speed estimation algorithm is developed by utilizing the autocovariance function of the received signal power, and a low pass finite impulse response (FIR) filter is introduced to suppress the high frequency noise and interference components. Specifically, the algorithm is tailored for EDGE system, and slot autocovariance function is introduced to avoid the slot burst frequency of EDGE system, which might affect the estimation accuracy. Both computer simulation and theoretical analysis show that the proposed mobile speed estimation algorithm is reliable, efficient, and it can be employed in a wide range of wireless communication system with diverse wireless environments.

TABLE OF CONTENTS

LIST OF FIGURES

LIST OF TABLES

CHAPTER 1

INTRODUCTION

1.1 Background and Motivation

In a modern communication system, the service area is divided into many cells. Each cell only covers a small portion of the total service area, and its base station, which communicates with all the mobile stations in the cell, uses different channels with the neighboring base stations. When a mobile station moves from one cell to another cell, the communication between the mobile station and current base station will be transferred to the new base station, and this process is called handoff. The handoff operation not only involves identifying a new base station, but also requires the allocation of new channels associated with the new base station. During a handoff, a call will be dropped if there is no available channel in the new cell, or the handoff takes too long that current base station cannot assist the conversation. Apparently, fewer handoffs reduce the burden of the system, thus result in better performance.

In practical cellular systems, high-speed vehicles and low-speed pedestrians usually appear in the same cell. The vehicles pass through cells very quickly, while the pedestrians may never walk out a cell during a phone call. In this case, handoffs happen frequently for vehicles but are rare for pedestrians. To cope with this phenomenon, the hierarchical wireless network is introduced. By using antenna placed at different heights and working at different power levels, it is possible to have several smaller cells nested in

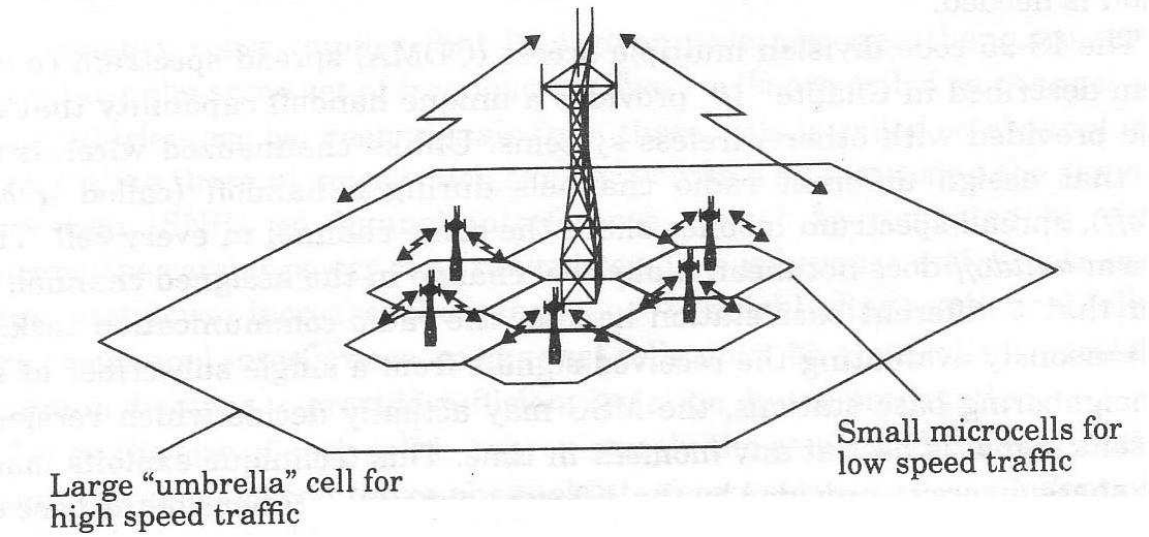

Figure 1-1 The umbrella cell approach.

one bigger cell, which is the so called "umbrella cell" approach as illustrated in Figure 1-1. An umbrella cell includes several microcells overlaid by one macrocell, where microcells provide small coverage to slow moving users and macrocell provides large coverage for high-speed mobiles. By this means, umbrella cell reduces the number of handoffs incurred by high-speed users.

The proper functioning of the hierarchical cellular structure are based on the assumption that the base station or the mobile switching center (MSC) have the ability of classifying mobile users based on their respective speeds. Therefore in the hierarchical wireless network, reliable speed estimation is desirable. Based on the estimated speed, the mobile users will be classified as either high-speed user or low-speed user, and the results will be used to assist hierarchical cell assignment.

1.2 Objective

This thesis work focuses on the development of reliable and fast mobile speed estimation algorithm for practical wireless information system with a wide range of system configurations. The objective lies in three aspects. First of all, the algorithm must be highly reliable, which means it should be able to correctly decide the mobile speed range with a very low rate of decision errors. Only with reliable speed estimation algorithm can the base station or MSC make proper cell assignments to different mobile users based on their respective moving speeds. Second, the speed estimation algorithm must be fast and easy to implement in practical wireless communication systems. The base station or MSC usually needs to make the cell assignment decision in a very short period of time. If the algorithm is too complicated, then a lot of CPU time will be consumed by the speed estimation, thus reduce the overall system efficiency. On the other hand, with simple algorithm, it will be easily implemented in hardware, and the time used for speed estimation will be significantly shorter. Finally, the algorithm must be applicable to a wide range of wireless environments. Due to the wireless nature of the propagation environments, the properties of the channel through which the signals are transmitted change dramatically at different locations. The mobile speed estimation algorithm should be able to cope with these diverse wireless environments to make correct classifications without the prior knowledge of the statistical distributions of the wireless signals.

To facilitate the mobile speed estimation algorithm design, the statistical properties of various wireless propagation environments, such as Rayleigh fading, Rician fading, flat fading and frequency selective fading, are analyzed. The analytical results are then employed in the mobile speed estimation algorithm design. The three aspects of the

design objective are treated as important factors during the development of the new mobile speed estimation algorithm.

1.3 Review of Other Mobile Speed Estimation Algorithms

Several methods exist in the literature for mobile speed estimation **[1]** – **[5]**. These methods can be roughly classified into three categories.

First, in **[1]**, the mobile speed range is estimated by computing the squared deviation of the received signal envelope or logarithm of the signal envelope. The squared deviation of the signal envelope is proportional to the slope of the signal variation, which is in turn related to the mobile speed. The algorithms are simple and easy to implement, and it is independent of Rayleigh or Rician fading channel. However, they do not work well under frequency selective fading channel.

Second, the mobile speed is estimated with the estimation of the maximum Doppler spread of the wireless fading channel **[2]**. For wireless communication system with fixed carrier frequency, the maximum Doppler spread of the fading channel is uniquely determined by the mobile speed. Thus if the maximum Doppler spread can be correctly identified at the communication receiver, then the mobile speed can be easily computed based on their relationship. In **[2]**, the maximum Doppler spread is estimated by analyzing the spectrum of the received signals. The reliability of this method will be compromised if there are multiple local maximum in the spectrum of the fading process, and this is possible for frequency selective fading channels.

The third category of mobile speed estimation algorithms are based on the correlation function of the received signals. In **[3]**, the mobile speed of users in flat fading channel is estimated by analyzing the correlation function of the received signal. In **[4]** and **[5]**, the

power auto-correlation function of the received signal is employed for the speed estimation of users in both flat and frequency selective fading channel. Both of the two algorithms work only under Rayleigh fading environment.

1.4 Thesis Outline

The remaining of the thesis is organized as follows.

Chapter 2 builds up the theoretical foundations necessary for mobile speed estimation algorithm development. The relationship between the mobile speed and the Doppler frequency of the communication channel is investigated. We then described various fading channels and their statistical properties. Specific emphases are given to the auto-correlation function and autocovariance, which are closely related to the maximum Doppler spread of the fading channel.

Chapter 3 develops a new mobile speed estimation algorithm for system with both Rayleigh and Rician fading channels. Based on the statistical fading properties obtained in Chapter 2, the algorithm is developed by analyzing the autocovariance functions of the squared envelope (power) of the received signal. The formulation and procedures of this algorithm are described in details. Moreover, it's shown that a single algorithm can be used for the speed estimation in both Rayleigh and Rician, flat and frequency selective fading environments.

Chapter 4 presents the application of this new mobile speed estimation algorithm in EDGE (Enhanced Data rates for GSM Evolution) system, which is a candidate for the next generation wireless communication system. The modulation scheme, slot structure, frame structure and other parameters adopted by EDGE system are introduced. The mobile speed estimation algorithm is tailored based on these specific system

configurations such that it will work in EDGE systems. Moreover, a low-pass finite impulse response (FIR) is introduced in the algorithm for noise and interference cancellation, and it is used to improve the mobile speed estimation accuracy.

Chapter 5 describes the construction and configuration of a baseband simulator for EDGE system. The modulator, pulse-shaping filter, channel simulation model, co-channel interference and additive noise are described in details. The simulator will be used for the performance evaluation of the mobile speed estimation algorithm.

Chapter 6 demonstrates the performance of the proposed mobile speed estimation algorithm with simulation results. With the EDGE system simulator described in Chapter 5, the mobile speed estimation algorithm is applied to system with various wireless propagation environments. The validity of the algorithm is verified by the simulation results.

Chapter 7 concludes the thesis.

CHAPTER 2

PROPERTIES OF FADING CHANNELS

2.1 Introduction

Usually there is not only one propagation path between the mobile station and base station because of the nature and man-made objects that surround the mobile station. As a consequence of reflection, scattering and diffraction, multiple versions of the transmitted signal arrive at a mobile station from different directions with different delays. The multiple waves, called multipath waves, combine vectorially at the receiver antenna to produce a composite received signal.

The composite received signal may consist of a large number of plane waves having randomly distributed amplitudes, phases, and angles of arrival. These multipath components could add up either constructively or destructively at the receiver, and cause the received signal distort or fade.

Due to the relative motion between the mobile and base station, each multipath wave experiences an apparent shift in frequency, which is called the Doppler shift. Doppler shift is directly proportional to the velocity of the mobile with respect to the direction of arrival of the received multipath wave.

The primary purpose of this chapter is to discuss how mobile movement affects the fading channel and to review some principal characteristics and statistical properties of fading channels. The concept of Doppler shift is introduced in next section. The main

characteristics and classification of fading channels are presented in Section 2.3. The statistical properties of different fading channels are described in Section 2.4.

2.2 Doppler Shift

The relative movement between the base station and the mobile station introduces Doppler shift, which is a frequency shift in the propagation signals. The value of the Doppler shift is given by

$$f_D = f_M \cos\theta, \tag{2.1}$$

where θ is the incident angle between the direction of the motion of the mobile and the direction of the arrival of the signal wave as shown in Figure 2-1, and f_M is the maximum Doppler shift, which is defined by

$$f_M = \frac{v}{\lambda}, \tag{2.2}$$

where *v* is the speed of the mobile station, λ is the wavelength of the arriving wave. The signal wavelength λ can be expressed by

$$\lambda = \frac{c}{f_c}, \tag{2.3}$$

where $c = 3.0\times10^8$ m/s is the speed of light, and f_c is the carrier frequency of the wireless communication system. Given carrier frequency f_c, the maximum Doppler shift f_M is uniquely determined by the speed of the mobile station as defined in (2.2) and (2.3). Therefore, the mobile speed *v* can be estimated by identifying the maximum Doppler shift of the fading channel.

Doppler shift results in the time variation of the communication channel. The larger the Doppler frequency is, the faster the channel changes in a given time period. By analyzing

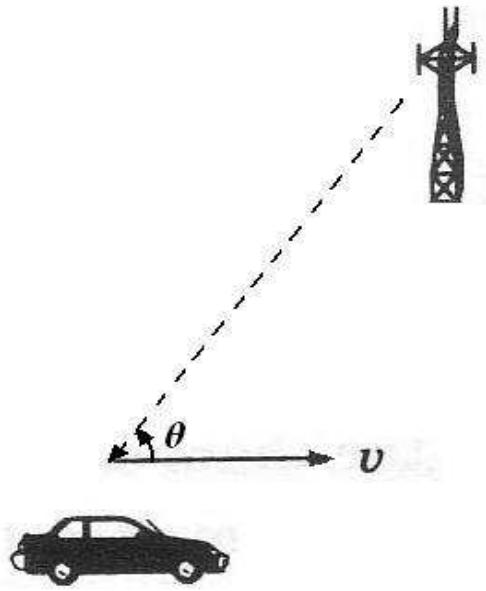

Figure 2-1 Illustration of Doppler effect.

the statistical properties of the fading channel in time domain, we can estimate the Doppler shift inherent in the channel, thus the corresponding mobile speed can be found out.

The statistic properties of the time varying fading channel at different environments are analyzed in the following.

2.3 Classification of Fading Channels

Multipath fading can be classified based on different classification criterions.

By comparing the rate of change of the transmitted signal and the mobile radio channel, a channel may be classified either as a fast fading channel or a slow fading channel. The changing rate of a fading channel can be measured by its coherence time in the time domain, which is defined as the time span over which the statistical fading is correlated.

In fast fading channel, the channel changes faster than the transmitted signal, that is, the impulse response of the channel changes rapidly within the symbol duration of the transmitted signal. On the other hand, if the channel changes slower than the transmitted signal, which means the coherence time of the channel is larger than the symbol period of the transmitted signal, the channel is experiencing slow fading.

The time domain variation of the mobile radio channel is introduced by the relative movement between the transmitter and receiver, thus the channel's rate of change can also be measured by Doppler spread in the frequency domain. As discussed before, Doppler spread of a fading channel is proportional to the relative speed between base station and mobile station. The larger the Doppler spread is, the faster the channel changes.

Multipath transmission leads to time delay spread in the communication channel. Delay spread is introduced by the relative propagation delays among radio waveforms. Delay spread characterizes the fading channel coherence bandwidth, which is defined as the frequency range over which the fading is correlated. Depending on the comparison between the time dispersion of the channel and the symbol period of the transmitted signal, a channel may be specified as flat fading or frequency selective fading channel. If the time domain delay spread of the channel is smaller than the symbol period of the transmitted waveform, the transmitted signal undergoes flat fading. The channel creates frequency selective fading over the received signal if the channel has a constant gain and linear phase response over a bandwidth that is smaller than the bandwidth of the transmitted signal, i.e., the coherence bandwidth of the fading channel is smaller than the signal bandwidth.

In mobile radio channels, the received signal often consists of a specular signal component, such as a direct line of sight (LOS) propagation path. In this case, the envelope of the received signal follows Rician distribution, and the fading is called Rician fading. When there is no direct LOS between the mobile station and the base station, the fading envelope distribution obeys Rayleigh distribution, and the fading channel is called Rayleigh fading channel.

Different classifications can be applied to one same channel. For example, when both of the coherence time and the delay spread of the channel are greater than the symbol period of the transmitted signal, and there is a LOS component in the received signal, the mobile radio channel is a slow time-varying, frequency selective, Rician fading channel.

2.4 Statistical Properties of Fading Channels

Since the mobile speed, or the Doppler spread, is directly related to the rate of time domain variation, we are going to investigate the time domain statistical properties of various fading channels.

2.4.1 Flat Fading

Consider the transmitted band-pass signal

$$s(t) = \mathrm{Re}\{\tilde{s}(t)e^{2\pi f_c t}\}, \tag{2.4}$$

where $\tilde{s}(t)$ is the complex envelope of the transmitted waveform, f_c is the carrier frequency, and $\mathrm{Re}\{z\}$ denotes the real part of z. The nth path of the received noiseless band-pass signal is

$$r_n(t) = \mathrm{Re}\{\alpha_n e^{j2\pi[(f_c+f_D)(t-\tau_n)]}\tilde{s}(t-\tau_n)\}, \tag{2.5}$$

where α_n and τ_n are the amplitude and time delay of the *n*th propagation path of the mobile radio channel, and f_D is Doppler frequency, which is incurred by the relative movement between base station and mobile station.

If the channel is comprised of *N* paths, then the received band-pass signal $r(t)$ can be expressed by

$$r(t) = \mathrm{Re}\{\sum_{n=1}^{N} \alpha_n e^{j2\pi[(f_c+f_D)(t-\tau_n)]} \tilde{s}(t-\tau_n)\}$$

$$= \mathrm{Re}\{\tilde{r}(t) e^{2\pi f_c t}\}, \tag{2.6}$$

where the received complex low-pass signal $\tilde{r}(t)$ is

$$\tilde{r}(t) = \sum_{n=1}^{N} \alpha_n e^{-j2\pi[(f_c+f_D)\tau_n - f_D t]} \tilde{s}(t-\tau_n). \tag{2.7}$$

The signal $\tilde{r}(t)$ can be alternatively written as

$$\tilde{r}(t) = \sum_{n=1}^{N} \alpha_n e^{j\phi_n(t)} \tilde{s}(t-\tau_n), \tag{2.8}$$

where

$$\phi_n(t) = -2\pi\{(f_c + f_D)\tau_n - f_D t\} \tag{2.9}$$

is the phase associated with the *n*th path.

Based on (2.8), the time-varying impulse response of the fading channel can be written as

$$h(t,\tau) = \sum_{n=1}^{N} \alpha_n e^{j\phi_n(t)} \delta(\tau-\tau_n), \tag{2.10}$$

where *t* represents the time variation of the channel, and τ corresponds to the propagation delay of the multipath radio waves. $h(t,\tau)$ can be interpreted as the response of the channel at time *t* to an impulse input at the time instant of $t-\tau$ **[6]**.

For flat fading channel, the maximum delay spread of the channel is far less than the symbol period, or $|\tau_i - \tau_j| \ll T_s,\ \forall i, j \in [1, 2, \cdots, N]$, where T_s is the symbol period of the transmission signal. In this case, all the multipath components can be treated as arriving at approximately the same time instant, thus it's sufficient to analyze the statistical properties of the fading channel only in the time domain *t*. The time-varying channel impulse response of flat fading channel can be represented by

$$g(t) = \sum_{n=1}^{N} \alpha_n e^{j\phi_n(t)}. \tag{2.11}$$

The baseband representation of the fading channel can be written in quadrature form as

$$g(t) = g_I(t) + jg_Q(t), \tag{2.12}$$

where

$$g_I(t) = \sum_{n=1}^{N} \alpha_n \cos\phi_n(t) \tag{2.13}$$

and

$$g_Q(t) = \sum_{n=1}^{N} \alpha_n \sin\phi_n(t) \tag{2.14}$$

represent the in-phase component and the quadrature component of the complex signal, respectively. According to equation (2.6), the received band-pass signal can be expressed by

$$r(t) = g_I(t)\cos 2\pi f_c t - g_Q(t)\sin 2\pi f_c t. \tag{2.15}$$

For common wireless propagation environment, the number of multipath components, or *N*, is usually very large. According to central limit theorem **[7]**, $g_I(t)$ and $g_Q(t)$ are Gaussian distributed.

When there is no LOS path between the transmitter and receiver, the quadrature component $g_I(t)$ and in-phase component $g_Q(t)$ are zero-mean Gaussian distributed. The envelope of the fading, which is $|g(t)| = \sqrt{g_I^2(t) + g_Q^2(t)}$, is Rayleigh distributed with probability density function (pdf) given by **[8]**.

$$p(x) = \begin{cases} \frac{x}{\sigma^2} e^{-\frac{x^2}{2\sigma^2}} & (0 \le x \le \infty), \\ 0 & (x < 0) \end{cases} \tag{2.16}$$

where σ^2 is the variance of the Gaussian process $g_I(t)$ and $g_Q(t)$.

In this case, the channel is experiencing Rayleigh fading and has the following statistical properties:

The autocorrelation functions of the quadrature components are

$$R_{g_I g_I}(\tau) = \frac{\Omega_p}{2} J_0(2\pi f_M \tau), \tag{2.17}$$

$$R_{g_Q g_Q}(\tau) = R_{g_I g_I}(\tau), \tag{2.18}$$

where $\Omega_p = \sum_{n=1}^{N} \mathrm{E}[\alpha_n^2]$ is the total power of the fading signal, $J_0(x)$ is the zero-order Bessel function of the first kind, and f_M is the maximum Doppler frequency of the time-varying channel.

The cross-correlation functions of the quadrature components are

$$R_{g_I g_Q}(\tau) = 0, \tag{2.19}$$

$$R_{g_Q g_I}(\tau) = -R_{g_I g_Q}(\tau). \tag{2.20}$$

The autocorrelation function of the complex envelope of fading signal $g(t)$ is

$$R_{gg}(\tau) = R_{g_I g_I}(\tau) + jR_{g_I g_Q}(\tau). \tag{2.21}$$

The autocorrelation function of the squared envelope, i.e., the power, of the fading is

$$R_{|g|^2|g|^2}(\tau) = 4R^2_{g_I g_I}(0) + 4R^2_{g_I g_I}(\tau) + 4R^2_{g_I g_Q}(\tau). \tag{2.22}$$

The autocovariance of the fading signal's power is

$$\Phi_{|g|^2|g|^2}(\tau) = 4R^2_{g_I g_I}(\tau) + 4R^2_{g_I g_Q}(\tau). \tag{2.23}$$

Equations (2.17), (2.19), (2.21), (2.22) and (2.23) are derived in the Appendix section.

If there is a LOS path present between the transmitter and receiver, the envelope of the fading $|g(t)| = \sqrt{g_I^2(t) + g_Q^2(t)}$ obeys Rician distribution, the pdf of which is expressed as **[8]**

$$p(x) = \begin{cases} \frac{x}{\sigma^2} e^{-\frac{(x^2+A^2)}{2\sigma^2}} I_0\left(\frac{Ax}{\sigma^2}\right) & (0 \le x \le \infty) \\ 0 & (x < 0), \end{cases} \tag{2.24}$$

where σ^2 is the variance of $g_I(t)$ and $g_Q(t)$, A is the maximum amplitude of the dominant (LOS) signal, and $I_0(x)$ is the modified zero-order Bessel function of the first kind.

Here, the channel is experiencing Rician fading and has the following statistical properties:

The autocorrelation functions of the quadrature components are

$$R_{g_I g_I}(\tau) = \frac{1}{K+1}\frac{\Omega_p}{2} J_0(2\pi f_M \tau) + \frac{K}{K+1}\frac{\Omega_p}{2}\cos(2\pi f_M \tau \cos\theta_0), \tag{2.25}$$

$$R_{g_Q g_Q}(\tau) = R_{g_I g_I}(\tau), \tag{2.26}$$

where $\Omega_p = \sum_{n=1}^{N} \mathrm{E}[\alpha_n^2]$ is the total power of the fading, $J_0(x)$ is the zero-order Bessel function of the first kind, K is called the Rician factor and is defined as the ratio of the specular power to the power of the scattering components, and θ_0 represents the angle of arrival (AoA) of the LOS propagation path.

The cross-correlation functions of the quadrature components are

$$R_{g_I g_Q}(\tau) = \frac{K}{K+1}\frac{\Omega_p}{2}\sin(2\pi f_M \tau \cos\theta_0), \tag{2.27}$$

$$R_{g_Q g_I}(\tau) = -R_{g_I g_Q}(\tau). \tag{2.28}$$

The autocorrelation function of the complex envelope of fading signal $g(t)$ is

$$R_{gg}(\tau) = R_{g_I g_I}(\tau) + jR_{g_I g_Q}(\tau). \tag{2.29}$$

The autocorrelation function of the squared envelope of fading signal is

$$R_{|g|^2|g|^2}(\tau) = \left(\frac{\Omega_p}{K+1}\right)^2 \left[1 + 2K + K^2 + J_0^2(2\pi f_M \tau) + 2KJ_0(2\pi f_M \tau)\cos(2\pi f_M \tau \cos\theta_0)\right]. \tag{2.30}$$

The autocovariance function of the fading signal's power is

$$\Phi_{|g|^2|g|^2}(\tau) = \left(\frac{\Omega_p}{K+1}\right)^2 \left[J_0^2(2\pi f_M \tau) + 2KJ_0(2\pi f_M \tau)\cos(2\pi f_M \tau \cos\theta_0)\right]. \tag{2.31}$$

Equations (2.25), (2.27), (2.30) and (2.31) are derived in the Appendix section.

2.4.2 Frequency Selective Fading

If the maximum delay spread of the propagation paths is larger than the symbol period of the transmitted signal, the channel exhibits frequency selective fading. The impulse response of time-varying frequency selective fading can be represented by

$$g(t,\tau) = \sum_{l=1}^{L} g_l(t)\delta(\tau - \tau_l) \tag{2.32}$$

where L is the number of resolvable paths, $g_l(t)$ and τ_l are the time-varying impulse response and relative delay of the lth resolvable path.

For system experiencing wide sense stationary uncorrelated scattering (WSSUS) **[6]**, we can write the two-dimensional autocorrelation function of the complex envelope $g(t,\tau)$ as

$$R_{gg}(\beta,\gamma)=\frac{1}{2}\mathrm{E}[g^{*}(t,\tau)g(t+\beta,\tau+\gamma)] \tag{2.33}$$

When there is no LOS component between the transmitter and receiver, $g_l(t)$, for l = 1, …, L, are zero-mean complex Gaussian distributed. Then the autocorrelation function of $g(t,\tau)$ can be derived as

$$\begin{aligned} R_{gg}(\beta,\gamma) &= \frac{1}{2}\mathrm{E}\left[\sum_{l_1=1}^{L} g_{l_1}^{*}(t)\delta(\tau-\tau_{l_1})\sum_{l_2=1}^{L} g_{l_2}(t+\beta)\delta(\tau+\gamma-\tau_{l_2})\right] \\ &= \frac{1}{2}\mathrm{E}\left[\sum_{l_1=1}^{L}\sum_{l_2=1}^{L} g_{l_1}^{*}(t)g_{l_2}(t+\beta)\delta(\tau-\tau_{l_1})\delta(\tau+\gamma-\tau_{l_2})\right]. \end{aligned} \tag{2.34}$$

If $l_1 \neq l_2$, $g_l(t)$ and $g_l(t)$ represent different propagation paths and they are independent, and their expectation equal to 0 since they are zero-mean complex Gaussian process. Therefore

$$\begin{aligned} R_{gg}(\beta,\gamma) &= \sum_{l=1}^{L}\frac{1}{2}\mathrm{E}\left[g_l^{*}(t)g_l(t+\beta)\right]\delta(\tau-\tau_l)\delta(\tau+\gamma-\tau_l) \\ &= \sum_{l=1}^{L} R_{g_l g_l}(\beta)\delta(\gamma). \end{aligned} \tag{2.35}$$

When a LOS path exists, the effect of the LOS path is included in $g_1(t)$ since the LOS path always has the shortest propagation delay compared to the scattering components. In this case, $g_1(t)$ is a non-zero mean complex Gaussian process, and $g_l(t)$, for l = 2, …, L,

are zero-mean Gaussian distributed. Then we can write the autocorrelation function of $g(t,\tau)$ into two parts as

$$R_{gg}(\beta,\gamma)=\frac{1}{2}\mathrm{E}\left[g_1^*(t)g_1(t+\beta)\delta(\tau-\tau_1)\delta(\tau+\gamma-\tau_1)+\sum_{l_1=2}^{L}\sum_{l_2=2}^{L} g_{l_1}^*(t)g_{l_2}(t+\beta)\delta(\tau-\tau_{l_1})\delta(\tau+\gamma-\tau_{l_2})\right]$$
$$=R_{g_1g_1}(\beta)\delta(\gamma)+\sum_{l=2}^{L}R_{g_lg_l}(\beta)\delta(\gamma)\,. \qquad (2.36)$$

From (2.35) and (2.36), we can see that the autocorrelation function of the fading complex envelope in frequency selective fading channel is the combination of the autocorrelation function of the fading complex envelope of every resolvable path in both cases. Thus, in the sense of the relationship between maximum Doppler spread and auto-correlation function, we can conclude that frequency selective fading channel has similar properties with its corresponding flat fading channels.

2.5 Conclusions

In this chapter, we investigated the relationship of the mobile speed and the Doppler frequency of the communication channel. We then described various fading channels and their statistical properties. With the above theories in hand, we are now ready to develop the speed estimation algorithms over these channels.

CHAPTER 3

SPEED ESTIMATION ALGORITHM

3.1 Introduction

As described in chapter 2, in a communication system that has a fixed carrier frequency f_c, the relative movement between the mobile and base station, i.e., the speed of the mobile station, determines the channel's maximum Doppler frequency f_M, which is associated with the time domain variation of the channel. The fast the mobile moves, the fast the channel changes. By looking at the statistical properties of the mobile radio channel in time domain, we can estimate the rate of change of the channel, and then the maximum Doppler frequency, thus the mobile speed.

Nowadays, angle-modulated signals are utilized in most communication systems, such as FM, π/4 DQPSK, GMSK, 8PSK and QPSK modulations for AMPS, IS-136 TDMA, GSM, EDGE and code division multiple access (CDMA) systems, respectively. In angle modulation, the information is only contained in the angle of the transmitted signal, and the average power of the transmitted signal remains unchanged. After the transmitted signal pass through the fading channel, the received signal is strictly proportional to the power of the fading channel. Therefore, by examining the time domain statistical property of the received signal's power, which possesses the time domain statistical property of the power of the fading channel, we can analyze the change rate of the channel and estimate the speed of the mobile station.

In the remaining of this chapter, different fading channels are first analyzed in Section 3.2 to seek a proper speed estimation algorithm, and then the details of the speed estimation algorithm are presented in Section 3.3.

3.2 Speed Estimation for Fading Channels

As discussed in Chapter 2, flat fading channel and frequency selective fading channel share similar time domain properties, but there are significant differences between the Rayleigh fading channel and Rician fading channel because of the existence of the LOS propagation path. So Rayleigh and Rician fading channels are analyzed separately in this section.

3.2.1 Speed Estimation for Rayleigh Fading Channel

As said in Section 3.1, we concern the statistical properties of the power of the received signal, which is the same thing as the statistical properties of the power of the fading channel, and it can be easily measured at the receiver. The time domain statistical properties of Rayleigh fading channels are described in Section 2.4.

Substitute (2.22) with (2.17) and (2.19), we can derive the autocorrelation function of the fading power for flat fading channel as

$$R_{|g|^2|g|^2}(\tau) = \Omega_p^2 + \Omega_p^2 J_0^2(2\pi f_M \tau) . \tag{3.1}$$

Figure 3-1 plots the normalized power autocorrelation of Rayleigh fading signals against the normalized time delay $f_M \tau$.

It can be seen from Figure 3-1 that for a given time delay τ, the fluctuation of the autocorrelation of the signal power decreases along with the increase of the maximum Doppler frequency f_M, and the autocorrelation decreases dramatically when f_M is

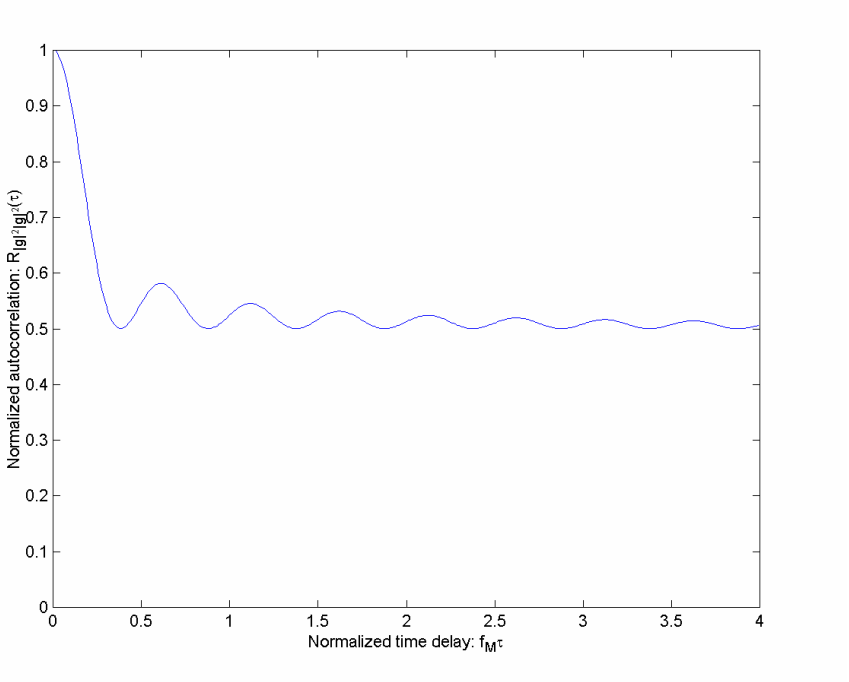

Figure 3-1 Normalized autocorrelation of the power of the Rayleigh fading signal in flat fading channel.

v (km/hr)	1	3	5	30	50	80	100	200
f_M (Hz)	1.7593	5.2778	8.7963	52.7778	87.9630	140.7407	175.9259	351.8519
$R_{\|g\|^2\|g\|^2}$	0.9993	0.9942	0.9839	0.6224	0.5027	0.5763	0.5104	0.5081

Table 3-1 Different maximum Doppler frequencies and normalized power autocorrelations corresponding to typical mobile speeds at $f_c = 1900$ MHz and $\tau = 4.615$ ms in flat Rayleigh fading channel.

relatively small, which implies the slow mobile speed. For example, suppose the time delay is the slot interval for the same user in EDGE system $\tau = 4.615$ ms, and the carrier frequency is $f_c = 1900$ MHz, when the mobile moves at speed v = 1km/hr, the maximum Doppler frequency $f_M = 1.7593$ Hz by (2.2), and the normalized power autocorrelation

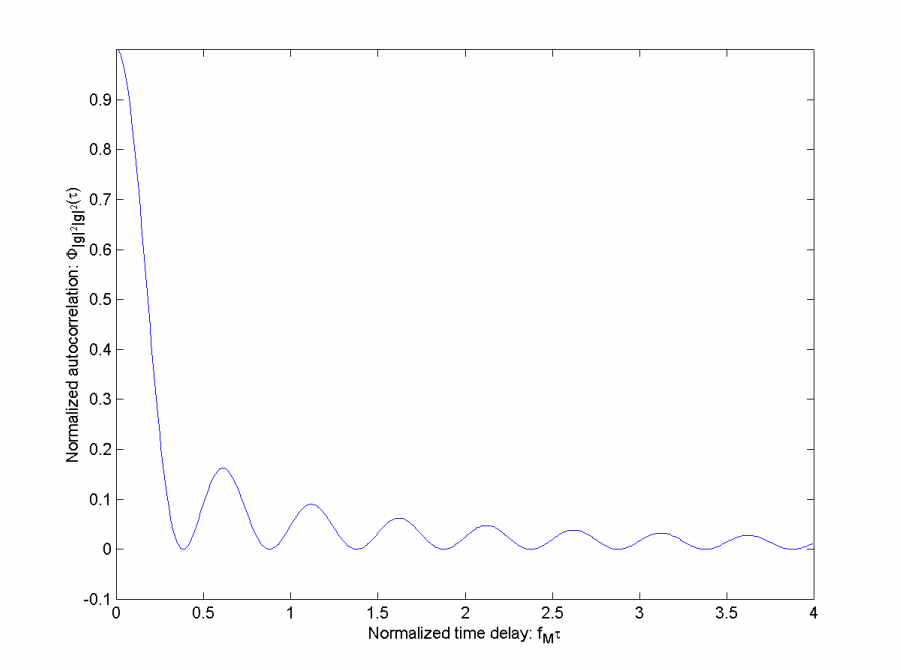

Figure 3-2 Normalized autocovariance of the power of the Rayleigh fading signal in flat fading channel.

v (km/hr)	1	3	5	30	50	80	100	200
f_M (Hz)	1.7593	5.2778	8.7963	52.7778	87.9630	140.7407	175.9259	351.8519
$\Phi_{\lvert g\rvert^2\lvert g\rvert^2}$	0.9987	0.9883	0.9679	0.2448	0.0054	0.1525	0.0207	0.0623

Table 3-2 Different maximum Doppler frequencies and normalized power autocovariances corresponding to typical mobile speeds at $f_c = 1900$ MHz and $\tau = 4.615$ ms in flat Rayleigh fading channel.

$R_{|g|^2|g|^2}$ is 0.9993 by (3.1). Table 3-1 lists some typical mobile speeds and their corresponding maximum Doppler frequencies and normalized power autocorrelation values.

From Table 3-1, we can see there is a big gap in power autocorrelation between the slow-moving mobiles ($v \le 5$ km/hr) and the fast-moving mobiles ($v \ge 30$ km/hr). If we set a

value in this gap as a threshold, it is easy to distinguish low- and high-speed mobiles by comparing their corresponding power autocorrelations to the threshold.

The autocovariance function of the fading power is given by (2.23), (2.17) and (2.19) as

$$\Phi_{|g|^2|g|^2}(\tau) = \Omega_p^2 J_0^2(2\pi f_M \tau), \tag{3.2}$$

and it is plotted in Figure 3-2.

For the above example with $f_c = 1900\,\text{MHz}$ and $\tau = 4.615\,\text{ms}$, Table 3-2 lists the maximum Doppler frequencies and normalized power autocovariance values corresponding to the typical mobile speeds.

Comparing Figure 3-2 to Figure 3-1 and Table 3-2 to Table 3-1, we find the gap between the slow-moving mobiles and the fast-moving mobiles in their autocovariance values is much bigger than in their autocorrelation values. As shown in Table 3-1, the autocorrelation gap between the slow- and fast-moving mobiles is around 0.36, while the autocovariance gap between them is about 0.72. Larger gap means clearer separation, so the mobile speed estimation will be more accurate by looking at its autocovariance value than by using its autocorrelation value.

3.2.2 Speed Estimation for Rician Fading Channel

The autocorrelation function and autocovariance function of the fading power for flat Rician fading channel are defined in Section 2.4 as

$$R_{|g|^2|g|^2}(\tau) = \left(\frac{\Omega_p}{K+1}\right)^2 \left[1 + 2K + K^2 + J_0^2(2\pi f_M \tau) + 2KJ_0(2\pi f_M \tau)\cos(2\pi f_M \tau \cos\theta_0)\right] \tag{3.5}$$

and

$$\Phi_{|g|^2|g|^2}(\tau) = \left(\frac{\Omega_p}{K+1}\right)^2 \left(J_0^2(2\pi f_M \tau) + 2KJ_0(2\pi f_M \tau)\cos(2\pi f_M \tau \cos\theta_0)\right), \tag{3.6}$$

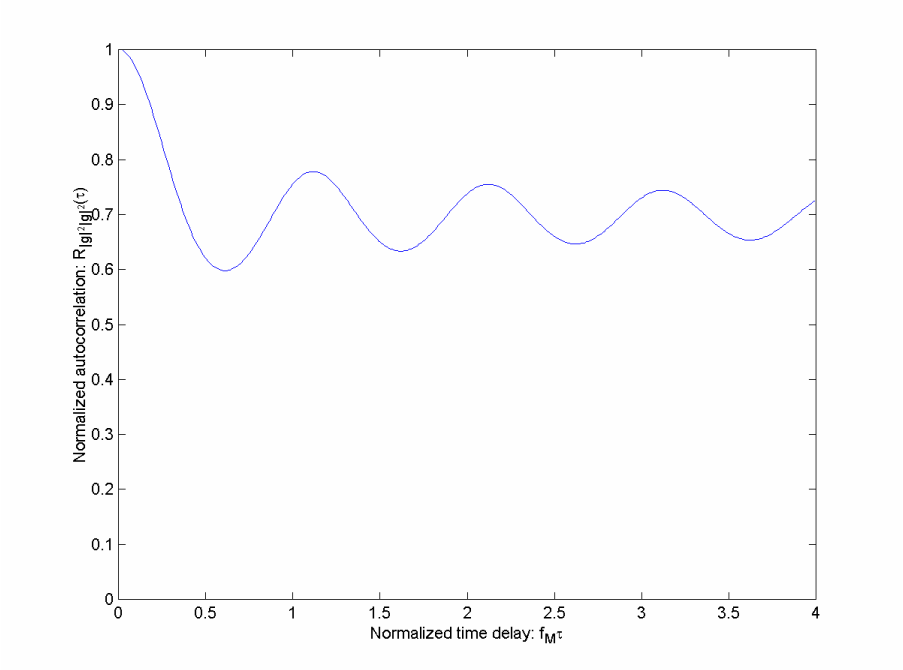

Figure 3-3 Normalized autocorrelation of the power of the Rician fading signal in flat fading channel.

v (km/hr)	1	3	5	30	50	80	100	200
f_M (Hz)	1.7593	5.2778	8.7963	52.7778	87.9630	140.7407	175.9259	351.8519
$R_{\lvert g\rvert^2\lvert g\rvert^2}$	0.9998	0.9980	0.9944	0.8354	0.6768	0.6004	0.6590	0.6332

Table 3-3 Different maximum Doppler frequencies and normalized power autocorrelations corresponding to typical mobile speeds at $f_c = 1900$ MHz and $\tau = 4.615$ ms in flat Rician fading channel.

If we set the Rician factor $K = 3$ and the LOS angle $\theta_0 = \frac{\pi}{2}$, the corresponding autocorrelation and autocovariance of the power of the Rician fading are plotted in Figure 3-3 and Figure 3-4, respectively. For the same example used in Rayleigh fading channel, we compute the corresponding autocorrelation and autocovariance values to some typical

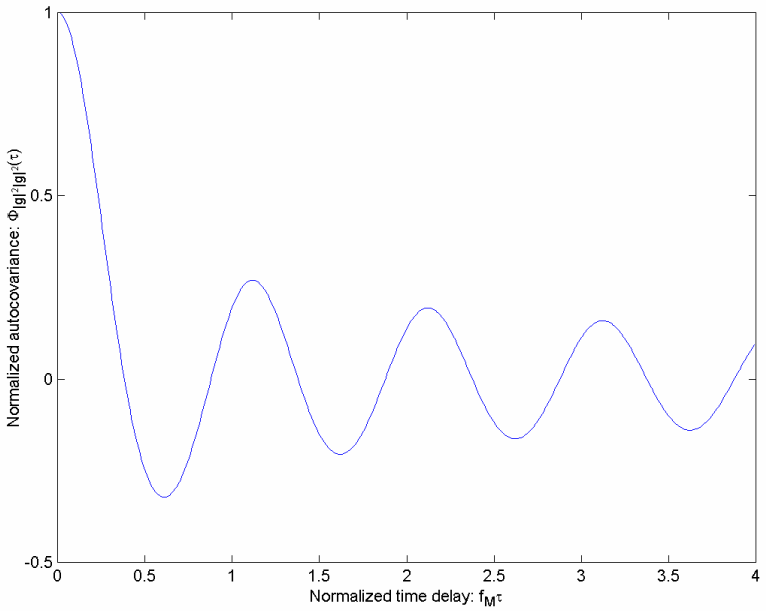

Figure 3-4 Normalized autocovariance of the power of the Rician fading signal in flat fading channel.

v (km/hr)	1	3	5	30	50	80	100	200
f_M (Hz)	1.7593	5.2778	8.7963	52.7778	87.9630	140.7407	175.9259	351.8519
$R_{\|g\|^2\|g\|^2}$	0.9993	0.9933	0.9815	0.4591	-0.0620	-0.3130	-0.1204	-0.2050

Table 3-4 Different maximum Doppler frequencies and normalized power autocovariances corresponding to typical mobile speeds at $f_c = 1900$ MHz and $\tau = 4.615$ ms in flat Rician fading channel.

mobile speeds at $f_c = 1900$ MHz and $\tau = 4.615$ ms, and the results are listed in Table 3-3 and Table 3-4.

It can be seen from Figure 3-3 and Table 3-3 that the difference of the fading power's autocorrelation between low-speed and high-speed mobiles is relatively small, and it is not sufficient to distinguish slow- and fast-moving users because these values will be

affected by additive noise and interference in practice. So we have to depend on the fading power's autocovariance, which demonstrates a much bigger gap between the low speed users and high-speed users, as shown in Figure 3-4 and Table 3-4, to estimate the speed of mobile stations.

3.2.3 Summary of Speed Estimation for Fading Channels

From the analysis of Rayleigh and Rician fading channel in Section 3.2.1 and 3.2.2, we can conclude that, for a given time difference τ, the values of autocorrelation and autocovariance of the fading channel power are relatively big when the mobile speed is low, and they become smaller for high-speed mobiles. This quantity difference between high-speed mobiles and low-speed mobiles is more distinct for the autocovariance function. So the mobile speed can be estimated by looking at the values of the autocovariance function of the fading channel power. For a certain time difference τ, if the autocovariance value of the fading power is relatively big, then the mobile is moving at a low-speed. Otherwise, the mobile has a high speed. Also it can be concluded from above sections that, although the autocorrelation and autocovariance functions of Rayleigh and Rician fading are different formulas, they have the similar shape and the same property, so we can use the same algorithm to estimate mobile speed for both of the Rayleigh and Rician fading channels.

3.3 Speed Estimation Algorithm

It is known **[9]** that for angle-modulated signal, a typical complex-valued baseband signal received at the base station is given by

$$v_R(k) = Am(k)r(k)e^{j[\omega_0 k+\varphi(k)+\phi(k)]} + \sum_i A_{I_i}(k)e^{j\varphi_i(k)} + \eta(k), \qquad (3.7)$$

where *A* is the amplitude of the transmitted signal, *m(k)* is the long-term shadow fading, *r(k)* is the short-term multipath fading, ω_0 the normalized carrier frequency offset between mobile and base station, $\varphi(k)$ is the transmitted angle-modulated signal, $\phi(k)$ is the Doppler phase, $A_{I_i}(k)$ is the time-varying amplitude of *i*th additive interference, and $\eta(k)$ is the complex-valued additive noise.

Then the power of the received signal is

$$s(k) = \left|v_R(k)\right|^2 = A^2 m^2(k) r^2(k) + \eta_{total}(k), \tag{3.8}$$

where $\eta_{total}(k)$ represents the total power of interference and noise. It can be seen that the carrier frequency offset ω_0 and the information-bearing signal $\varphi(k)$ are suppressed after the calculation of the power of the received signal.

Although the total interference and noise power $\eta_{total}(k)$ is only a small part of the received signal power *s(k)* because the carrier-to-interference radio (CIR) and carrier signal-to-noise ratio (SNR) are reasonably high when the mobile establishes communication with a base station, it makes the autocovariance of the received signal power become imprecise. Since we only interested in the Doppler spread, which is narrow-banded as usually between 0 to 500 Hz, we can pass the power of the received signal through a low-pass filter to remove the high-frequency interference and noise, and thus to calculate the autocovariance values more precisely. Let *h(k)* represents the impulse response of a selected finite impulse response (FIR) filter, then the filtered power signal is given by

$$s_F(k) = s(k) \otimes h(k), \tag{3.9}$$

where $\otimes$ is a convolution operator.

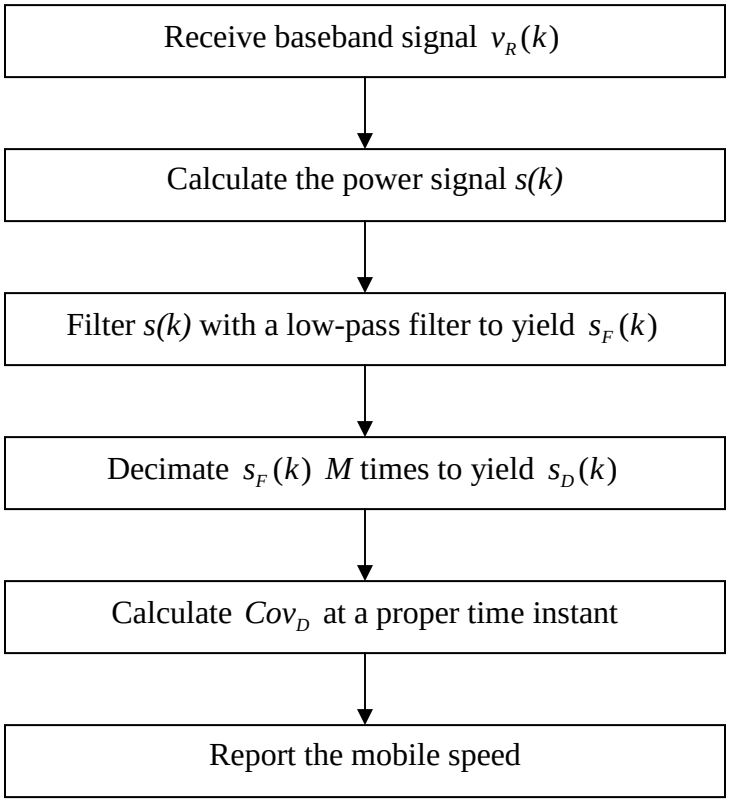

Figure 3-5 Signal flow of the new speed estimation algorithm.

The calculation of the power autocovariance of the received signal usually involves the computation of thousands of samples. To ease the computation burden, we can decimate the filtered power signals before calculate their autocovariance. Because usually the sample interval is so short that there is almost no difference between dozens of samples, the decimation will not influence the computation result. Let $s_D(k)$ be the *M* times decimated signal from $s_F(k)$, then we have

$$s_D(m) = s_F\left((m-1)M + i\right), \tag{3.9}$$

where $0 \le i \le M$. Assume the sampling frequency and the stop band edge frequency of the filter *h(k)* are f_T Hz and f_s Hz, respectively, the *M* shall not be larger than $f_T / 2 f_s$, otherwise the proposed decimation will have frequency aliasing **[10]**.

With the received signal being powered, filtered and decimated, we can calculate its autocovariance Cov_D by

$$Cov_D(n) = \sum_{l=1}^{N-n} \left(s_D(l+n) - \overline{s_D} \right) \left(s_D(l) - \overline{s_D} \right) \tag{3.10}$$

Where N is the total number of samples, and $\overline{s_D}$ is the average of $s_D(m)$. At a given n, larger the value of $Cov_D(n)$ means low-speed and vice versa. Figure 3-5 illustrates the procedure of the whole speed estimation algorithm.

3.4 Conclusions

A new speed estimation algorithm is presented in this chapter based on the analysis of fading channels. Although Rayleigh and Rician fading channels have different properties, they can employ the same algorithm to estimate the mobile speed. This algorithm can be used for both flat and frequency selective fading channels since these two kinds of channels have similar properties as discussed in Chapter 2.

CHAPTER 4

AN APPLICABLE SPEED ESTIMATION ALGORITHM FOR EDGE SYSTEMS

4.1 Introduction

EDGE is the acronym for Enhanced Data rates for GSM Evolution. The technology is part of the evolution from 2nd Generation networks to 3rd Generation networks and is often referred to as a 2.5G standard for mobile communication networks. EDGE improves the data capacity over global system for mobile communication (GSM), and enables the delivery of multimedia and other broadband applications to mobile users with its higher data transmission rate that is up to 384Kbps.

EDGE achieves the data speed enhancements by using eight-phase-shift keying (8PSK) signal modulation and making a better use of the carrier in good conditions. 8PSK modulation offers up to 48Kbps per channel, compared 9.6Kbps per channel for GSM with Gaussian minimum-shift keying (GMSK) modulation.

EDGE cellular system uses time division multiple access (TDMA) frame structure to allow up to eight users to use each of the channels. By allowing the simultaneous use of multiple channels, the technology allows rates of up to 384Kbps, using all eight channels.

Based on the properties of EDGE communication system, this chapter details the adapted speed estimation algorithm along with some specific parameters for EDGE system. Section 4.2 introduces slot autocovariance algorithm for EDGE system, and analyzes the

sample of slot autocovariance should be examined, and gives the thresholds of autocovariance used to estimate mobile speed. The number of slots used in the algorithm is stated in Section 4.3. Section 4.4 illustrates the employed low-pass FIR filter.

4.2 Slot Autocovariance

In EDGE systems, a mobile station sends voice/data slot by slot, and the duration of one slot is 576.9 μs. Since one channel supports 8 users simultaneously, the time from slot i to slot i+1 of the same mobile is 4.615 ms, which yields 217 Hz in the frequency domain and this frequency is referred to as "frame burst frequency" in this paper. The frame burst frequency is a strong potential interference to our mobile speed estimation, because it is inside the Doppler frequency range. To maximally eliminate this interference, we calculate the autocovariance values by frame basis only. Let $s_{Dl}(m)$ be *l*th-frame *m*th-sample of the decimated filtered power signal, and $\overline{s_D}$ be the average of the decimated filtered power signal sequence, then the autocovariance values of N frames are given by

$$Cov_D(n) = \sum_{l=1}^{N-n} \sum_{m=1}^{K_s/M} \left(s_{Dl+n}(m) - \overline{s_D}\right)\left(s_{Dl}(m) - \overline{s_D}\right), \qquad n = 0, 1, \ldots, N\text{-}1 \qquad (4.1)$$

where M is the decimation time, and K_s is the number of samples per slot to be considered. For example, K_s can be 156 in EDGE radios, and K_s/M should be an integer number. To minimize the power fluctuation factor, we normalize the autocovariance values as $Cov_D(n)/Cov_D(0)$.

In the autocovariance sequence we computed above, we need to pick a time instant, at which the autocovariance values of high- and low- speed mobiles can be easily

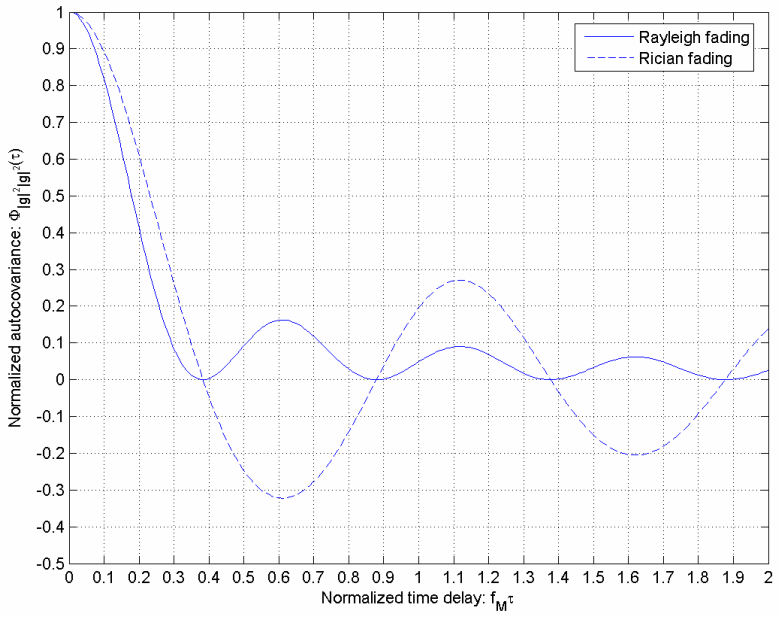

Figure 4-1 Normalized autocovariance of the power of Rayleigh and Rician fading signals in flat fading channel.

distinguished, so the mobile speed can be estimated by examining the corresponding autocovariance value at this time instant. As discussed in Chapter 2 and Chapter 3, the power autocovariance functions of Rayleigh fading channel and Rician fading channel have similar shape and the same properties. For comparison reason, Figure 4-1 plots the Rayleigh signal's power autocovariance along with the one of Rician signal in flat fading channel. In order to set the autocovariance value of high- and low-speed mobile apart, for example, to make $Cov_D(n)/Cov_D(0) > 0.8$ at $v \le 5$ km/hr and $Cov_D(n)/Cov_D(0) < 0.5$ at $v > 30$ km/hr, we'll need $f_M\tau < 0.1$ at $v \le 5$ km/hr and $f_M\tau > 0.24$ at $v \ge 30$ km/hr. It's known that the maximum Doppler frequency does not only depend on the mobile speed, but also depend on the carrier frequency regarding to (2.2) and (2.3), so a same mobile speed will generate different maximum Doppler frequencies in the EDGE system using

v (km/hr)		1	3	5	30	50	80	100	200
f_M (Hz)	$f_c = 1900$ MHz	1.7593	5.2778	8.7963	52.7778	87.9630	140.7407	175.9259	351.8519
	$f_c = 900$ MHz	0.8333	2.5000	4.1667	25.0000	41.6667	66.6667	83.3333	166.6667

Table 4-1 Corresponding maximum Doppler frequency f_M values of typical mobile speeds at $f_c = 1900$ MHz and $f_c = 900$ MHz.

1900MHz carrier frequency and the system with carrier frequency of 900MHz. Table 4-1 lists the values of maximum Doppler frequency f_M at various mobile speeds in both of the systems.

To satisfy $f_M \tau > 0.24$ at $v \geq 30$ km/hr in the system with $f_c = 1900$ MHz, we'll need $\tau > 0.0045$ s because the least value of f_M at $v \geq 30$ km/hr is 52.7778 Hz here. In EDGE system, the frame interval for the same mobile is 4.615 ms, which meets the requirement of $\tau > 0.0045$ s, and it also satisfies $f_M \tau < 0.1$ at $v \leq 5$ km/hr because the maximum f_M is 8.7963 in this case. So the first frame delay of 4.615 ms is a proper time instant to examine the normalized autocovariance value, which can be expressed by $Cov_D(1)/Cov_D(0)$. The delay of two frames, 9.23ms, satisfies the criteria and could be used as a proper time instant too, but the normalized autocovariance value $Cov_D(2)/Cov_D(0)$ for low-speed mobile at this time instant is smaller than the value at time instant 4.615 ms, and this reduces the difference between high- and low- speed mobiles. Therefore, in our algorithm, we'll use the normalized autocovariance value at time delay 4.615 ms (n=1) to evaluate the speed of mobile users in the EDGE system with carrier frequency at 1900 MHz.

For the EDGE system using carrier frequency $f_c = 900\,\text{MHz}$, following the same procedure, we can find 9.23ms, the time delay of two frames, is an appropriate time instant to study the normalized autocovariance value $Cov_D(2)/Cov_D(0)$.

Since flat fading channel and frequency selective fading channel have similar properties, as discussed in Chapter 2, above time delays can be applied not only the flat but also the frequency selective fading channel.

After the values of $Cov_D(1)/Cov_D(0)$ for 1900 MHz system or $Cov_D(2)/Cov_D(0)$ for 900 MHz system is obtained, we set two thresholds for low-speed mobile T_L and for high-speed mobile T_H with $T_L \geq T_H$, and estimate the mobile speed as follows: if the studied autocovariance value is larger than T_L, than the user is treated as slow-moving mobile; if the studied autocovariance value is smaller than T_H, then the mobile is fast-moving; if the studied autocovariance value is between T_L and T_H, then the mobile speed is indeterminate. The two thresholds can be set to $T_L = 0.8$ and $T_H = 0.5$, as the threshold we used to find the proper time instant. Consider the influence of noise and interference, we loosen the thresholds to $T_L = 0.65$ and $T_H = 0.55$ in our algorithm.

4.3 Number of Frames

EDGE radios uses TDMA scheme to support 8 users simultaneously in one channel by dividing a frame into 8 slots in time domain. The duration of one slot is 576.9 μs and the duration of one frame is 4.615 ms. In our algorithm, the autocovariance is computed based on the slots of one user as depicted in previous section, so the time spent for the mobile speed estimation is determined by how many slots used in the algorithm, and it is the same thing as the number of frames used because we assume one user only occupies

one slot in a frame here. Apparently using fewer frames makes the algorithm more efficient, but it also decreases the precision of the mobile speed estimation, especially when the mobile is moving very slowly. When the mobile speed is very low, the analyzing time duration is short, sometimes only a small part of the fading will be analyzed. At this time, the fading changes so little that it will be totally subtracted as the mean value when calculating its autocovariance, hence there is much less correlation in the remaining signal and the autocovariance becomes much smaller although it should be big. Therefore, the trade off is between the efficiency and the precision of the algorithm. We have to investigate many slots to ensure that we get enough statistics of the fading, while keep the waiting time tolerable. We choose 500 frames for our algorithm, and this brings the estimation result be reported by 2.3 s in real EDGE systems, because of the 4.615 ms frame duration.

4.4 Low-pass FIR Filter

It has been pointed out in Chapter 3 that a low-pass FIR filter could be used to remove the high-frequency interference and noise in the mobile speed estimation algorithm. EDGE cellular system transmits 156 samples in one slot and has 576.9 μs slot duration, so its sampling frequency F_s is 270 KHz. We select to pass its 5% bandwidth through the low-pass FIR filter. This survived 13.5 KHz bandwidth is wide enough to contain all the Doppler information we need, because the maximum Doppler frequency is about 415 Hz (850 Hz) when the mobile is traveling at 500 km/hr in the 900 MHz (1.9GHz) cellular cells. Figure 4-2 plots the low-pass linear phase FIR filter with 0.05 cut off frequency used in our algorithm.

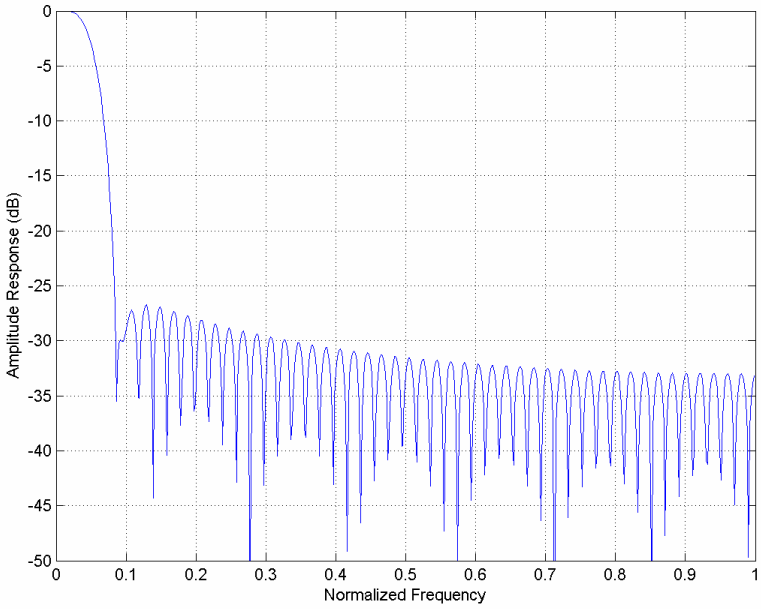

Figure 4-2 Amplitude response of the low-pass linear phase FIR filter.

At the receiver, the signals to be analyzed will first pass through the low pass FIR filter to get rid of high frequency interferences and noises. The output of the FIR filter will be used by the autocovariance based speed estimation algorithm.

4.5 Conclusions

This chapter introduces the concept of EDGE cellular system, and specifies some parameters and procedures for an applicable mobile speed estimation algorithm according to the properties of EDGE system. We compute the autocovariance of the signal power based on slots to avoid the slot burst frequency of EDGE system, and 500 slots are used to estimate one user's speed in our algorithm. With the low-pass FIR filter given to suppress the interference and noise, the proposed algorithm is completed and we'll apply it to a simulation model of EDGE system to see how the algorithm works.

CHAPTER 5

SIMULATION MODEL OF EDGE SYSTEMS

5.1 Introduction

Running tests in real communication systems could be extremely expensive, complicated and the test results are often hard to be reproduced. But with simulation models, we can finish our experiments in the laboratory, and it is less expensive and more reproducible than field trials.

Figure 5-1 demonstrates a simplified baseband EDGE system. The information bearing binary data are first modulated into symbols with 8PSK modulation scheme, and then passed through a pulse-shaping filter, in order to limit the bandwidth of the transmitted signal. When traveling through the communication channel, the transmitted signals are corrupted by fading, additive interferences and additive white Gaussian noise (AWGN). At the receiver, the received signal is reshaped by a matched filter and sampled at the symbol rate. After the 8PSK demodulation, the original binary data are recovered.

The mobile speed estimation is implemented after the sampling and before the 8PSK demodulation at the receiver. Hence our simulation model includes 8PSK modulation, shaping filter and matched filter, fading channels, additive interference and AWGN, and they will be described in the following sections of this chapter.

5.2 8PSK Modulation

Figure 5-2 shows the 8PSK modulation scheme. From the figure, we can see that 3 binary bits are mapped into one complex-valued symbol, which increases the transmitted data

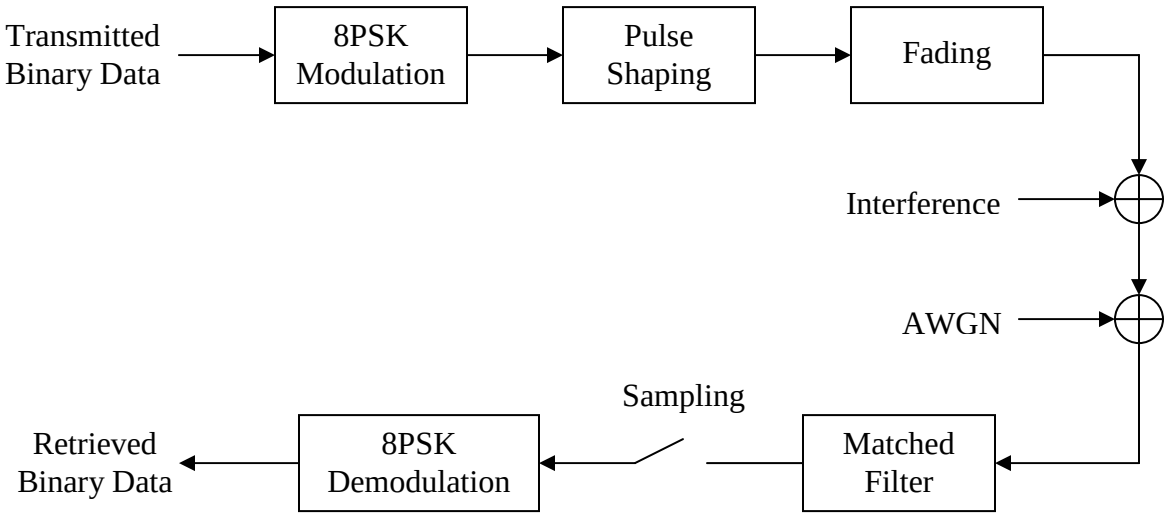

Figure 5-1 A simplified baseband EDGE system.

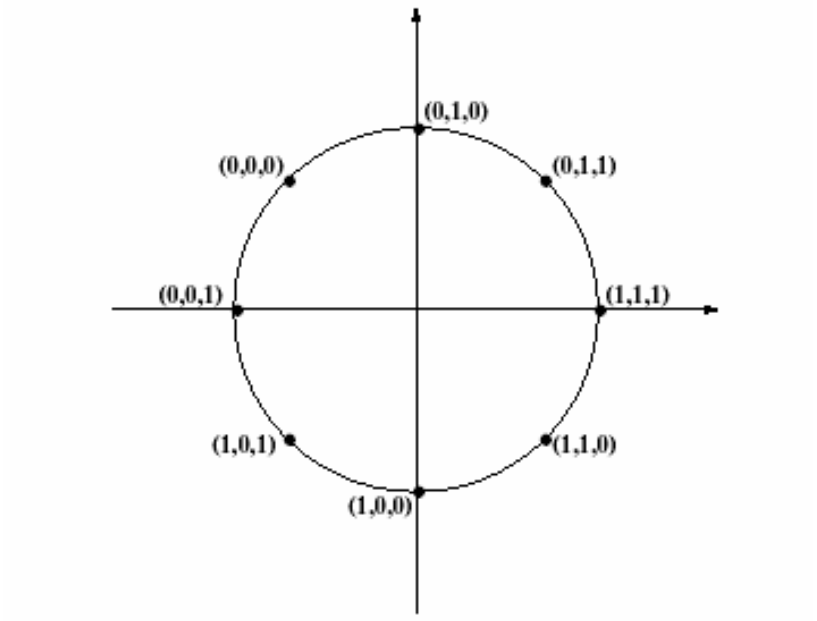

Figure 5-2 8PSK constellation.

rate and makes the system more efficient compared to other low level modulation schemes. 8PSK modulation generates 8 kinds of symbols, each symbol has different phase but the same amplitude. Also in 8PSK, in order to minimize the error bits generated in transmission, Gray code is used so that adjacent symbols have a single digit differing by 1.

5.3 Shaping Filter and Matched Filter

Before the transmitted signal is sent out to the channel, it is passed through a pulse-shaping filter to limit its bandwidth. Then at the receiver, a matched filter is used to restore the transmitted signal from the received signal.

We choose root raised cosine filter as our shaping pulse, and it is defined as

$$u(t) = \begin{cases} \frac{1}{\sqrt{T}} \frac{\sin[\pi(1-\alpha)t/T] + (4\alpha t/T)\cos[\pi(1+\alpha)t/T]}{(\pi t/T)[1-(4\alpha t/T)^2]} & t \neq 0, t \neq \pm\frac{T}{4\alpha} \\ \frac{1}{\sqrt{T}}\left[1-\alpha+\frac{4\alpha}{\pi}\right] & t = 0 \\ \frac{\alpha}{\sqrt{2T}}\left[(1+\frac{2}{\pi})\sin(\frac{\pi}{4\alpha}) + (1-\frac{2}{\pi})\cos(\frac{\pi}{4\alpha})\right] & t = \pm\frac{T}{4\alpha} \end{cases} \quad (5.1)$$

where T is the symbol period of the modulated signal, i.e., 3.7 μs in EDGE system, and α is the roll-off factor, which is set to 0.3 in our simulation model. To keep the energy of the transmitted signal unchanged after pass the shaping filter, the filter need to be normalized, as the total energy of the filter is 1. Figure 5-3 plots the shaping filter.

If we use *u(t)* to represent the shaping filter, then the matched filter should be represented by *u*(-t)*. Since the shaping filter is root raised cosine filter, which is real-valued and symmetric (5.1), we have *u*(-t) = u(t)*. Thus we are using exact the same shaping filter as the matched filter. And the same normalization is also required for the matched filter.

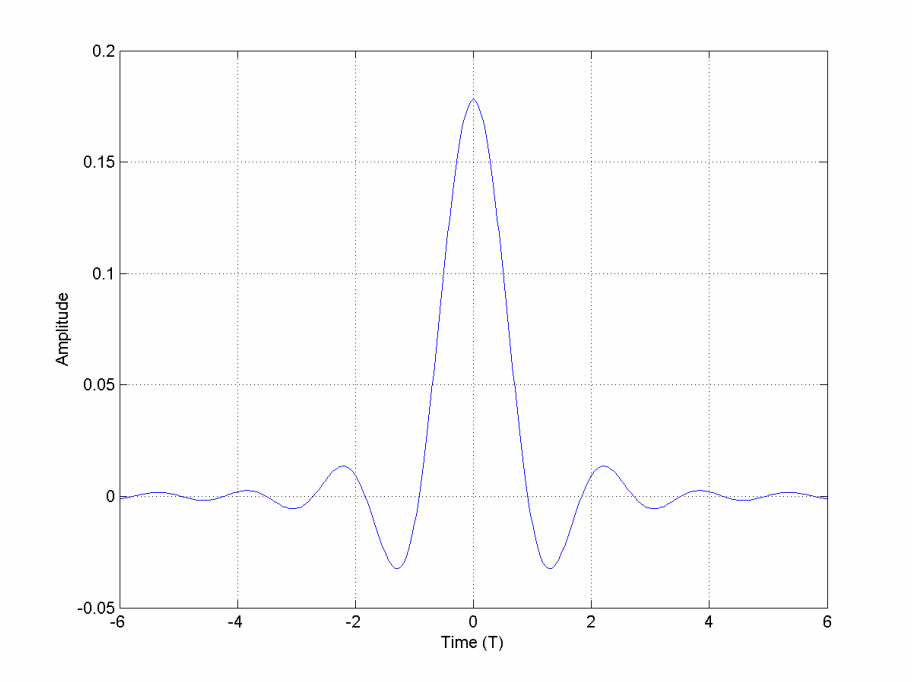

Figure 5-3 Root raised cosine filter at roll-off factor $\alpha = 0.3$.

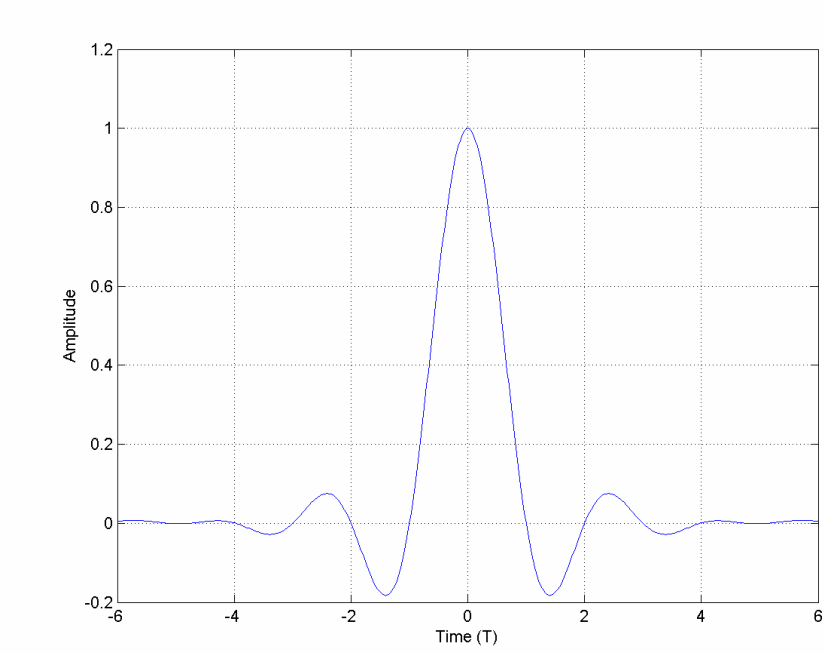

Figure 5-4 Convolution of shaping filter and matched filter.

The convolution result of the shaping filter and the matched filter is plotted in Figure 5-4, from which we can see that the use of shaping filter and matched filter will not introduce inter-symbol interference (ISI) in the transmitted signal.

5.4 Fading Channel

5.4.1 Rayleigh Fading

The simulation model of Rayleigh fading is given by

$$\begin{aligned} Y(t) &= Y_c(t) + jY_s(t) \\ Y_c(t) &= \sqrt{\frac{1}{N}} \sum_{n=1}^{N} \cos(\omega_d t \cos\alpha_n + \phi_n) \\ Y_s(t) &= \sqrt{\frac{1}{N}} \sum_{n=1}^{N} \cos(\omega_d t \sin\alpha_n + \phi_n) \end{aligned} \tag{5.2}$$

with

$$\alpha_n = \frac{2\pi n - \pi + \theta_n}{N}, \quad n = 1, 2, \ldots, N, \tag{5.3}$$

where N is the number of propagation paths, ω_d is the maximum radian Doppler frequency, α_n and ϕ_n are, respectively, the angle of arrival and initial phase of the nth propagation path. Both ϕ_n and θ_n are statistically independent and uniformly distributed over $[-\pi, \pi]$ for all n. The statistical properties of this simulator are the same as those of the theoretical Rayleigh fading we discussed in Chapter 2. **[11]**

5.4.2 Rician Fading

The Rician fading simulator just adds a specular component to the Rayleigh fading model, and it is defines as

$$
\begin{aligned}
Z(t) &= Z_c(t) + jZ_s(t) \\
Z_c(t) &= \left[Y_c(t) + \sqrt{K}\cos(\omega_d t \cos\theta_0 + \phi_0) \right] / \sqrt{1+K} \\
Z_s(t) &= \left[Y_s(t) + \sqrt{K}\sin(\omega_d t \cos\theta_0 + \phi_0) \right] / \sqrt{1+K}
\end{aligned}
\tag{5.4}
$$

where K is the ratio of the specular power to scattered power, θ_0 and ϕ_0 are the angle of arrival and the initial phase, respectively, of the specular component, and ϕ_0 is a random variable uniformly distributed over [$-\pi$, π]. This Rician fading simulation model has the same statistical properties as those of the theoretical Rician fading we discussed in Chapter 2. **[11]**

5.5 Additive Interference

Although the neighboring cellular cells use different frequencies as of current cell, some cells further away transmit signals in the same frequency range, and these signals may reach current cell and become additive interferences to our transmitted signal. This kind of interference is also called co-channel interference. Usually there is not only one co-channel interference exists in the radio channel, several interferences will present from different cells using the same carrier frequency.

The effect of additive interference can be quantized using carrier-to-interference ratio (CIR), which is a comparison of the signal energy, represented by *S*, and the total energy of all interferences, represented by *I*,

$$
CIR(dB) = 10\log_{10}\left(\frac{S}{I}\right). \tag{5.5}
$$

Usually CIR is 15 dB in practical systems.

5.6 Additive White Gaussian Noise (AWGN)

When the transmitted signal travels through the wireless channel, AWGN is linearly added to the signal. AWGN sequence consists of statistically independent, identically distributed, Gaussian random variables with zero-mean and σ^2 as variance. AWGN contains energy at all frequencies with equal power level at each frequency, which is the so-called flat spectrum. With our speed estimation algorithm, the noise at high frequencies will be eliminated by the low-pass FIR filter.

Suppose *S* denotes the signal energy, which is set to unit value in our simulation, and $N=\sigma^2$ denotes the noise energy, then we'll have the signal-to-noise ratio (SNR) computed by

$$SNR(dB) = 10\log_{10}\left(\frac{S}{N}\right) = 10\log_{10}\left(\frac{1}{\sigma^2}\right). \tag{5.6}$$

Most real EDGE systems have 15 dB SNR.

5.7 Conclusion

In our EDGE simulator, the binary data are generated and modulated by 8PSK modulation, and passed through the pulse-shaping filter to limit the bandwidth, and then the signal is transmitted into radio channel, at where the interferences and noises are added to the signal. We'll apply our speed estimation algorithm right after the received signal recovered from the matched filter. The simulation results will be presented in next chapter.

CHAPTER 6

SIMULATION RESULTS OF SPEED ESTIMATION FOR EDGE SYSTEMS

6.1 Introduction

In this chapter, we are going to apply the mobile speed estimation algorithm for EDGE systems depicted in Chapter 4 to the simulation model of EDGE systems described in Chapter 5. 500 slots are used to calculate the slot-based autocovariance and to estimate the speed of a mobile station. Each slot has 156 symbols, and we'll decimate them by 26 times for autocovariance computation, that means we'll investigate 6 samples of one slot. As discussed during the introduction of our algorithm in Chapter 4, we'll examine the autocovariance value at one frame delay (4.615 ms) for 1900 MHz EDGE systems, and the autocovariance at two-frame delay (9.23 ms) for 900 MHz EDGE systems. Both of the CIR and SNR are set to 15 dB in this chapter unless otherwise stated. The threshold of low-speed (speed $\leq$ 5 km/hr) mobiles is set to 0.65, and 0.55 is the threshold of high-speed (speed $\geq$ 30 km/hr) mobiles.

The simulations are performed under Rayleigh fading channel and Rician fading channel, flat and frequency selective fading channels. Section 6.2 presents the simulation result of EDGE systems with Rayleigh fading channel, in flat condition and frequency selective conditions, for both of the 900 MHz and 1900 MHz systems. Section 6.3 presents the simulation result of EDGE systems with Rician fading channel, in flat condition and

frequency selective conditions, for both of the 900 MHz and 1900 MHz systems. Some remarks and discussions about the simulation are described in Section 6.4.

6.2 Simulation results of Rayleigh Fading Channel

For convenient explanation, Figure 6-1 shows the calculated results of original power signals, filtered power signals, and decimated power signals in 900 MHz radio with flat Rayleigh fading channel, at mobile speed of 1, 3, 5, 30, 50, 80 and 200 km/hr. As can be seen from the figure, there is a gap between fast ($v \geq 30$ km/hr) and slow ($v \leq 5$ km/hr) mobiles. The filtered power signal's autocovariance value gives much better indication (wider gap) than the original power signals because some interferences and noises are eliminated by the low-pass filter, and the decimated filtered power signal's autocovariance gives almost the same size of the gap as the filtered power signals, so we can reduce the computation burden without degrade the estimation performance by decimating the filtered power signal before autocovariance calculation. Also from Figure 6-1, we can see that the gap at t = 9.23 ms, i.e. two-frame delay, is wide enough to distinguish the high-speed and low-speed mobiles from their autocovariance values of the filtered power signal or the decimated filtered power signal, this agrees with our speed estimation algorithm for 900 MHz EDGE system described in Chapter 4.

Now we take the normalized autocovariance value at n = 2 (t = 9.23 ms) and plot them into six sample speeds as shown in Figure 6-2, where solid lines stand for mean values, and then plot the probability density function of the decimated filtered power signal's autocovariance values in Figure 6-3. From these figures, it can be seen that the thresholds $T_L = 0.65$ and $T_H = 0.55$ we choose in our algorithm are capable of classifying slow- and fast-moving mobiles.

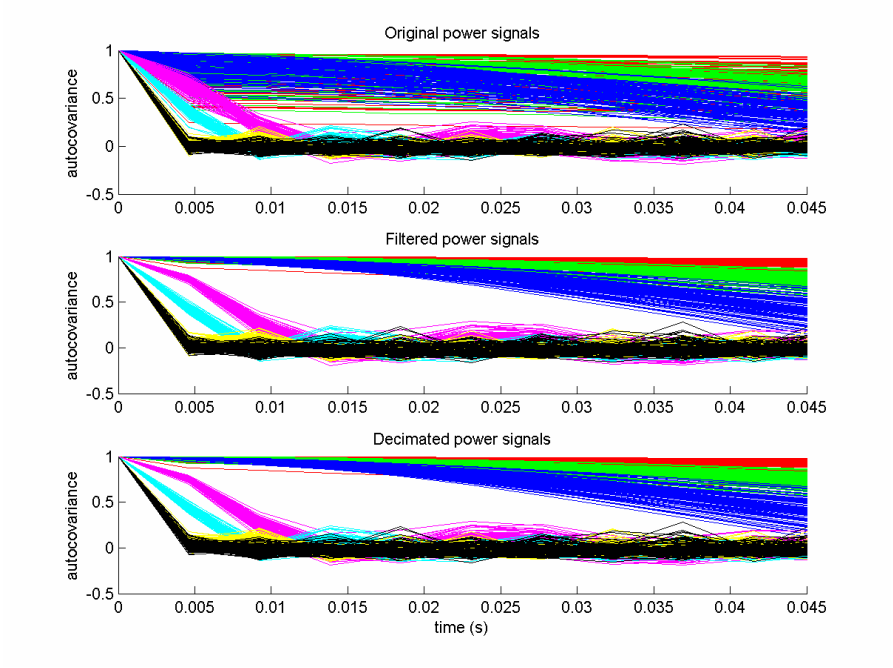

Figure 6-1 Autocovariance of 900 MHz EDGE system in flat Rayleigh fading channel, mobile speed = 1, 3, 5, 30, 50, 80 and 200 km/hr. (each speed shown 100 sample lines)

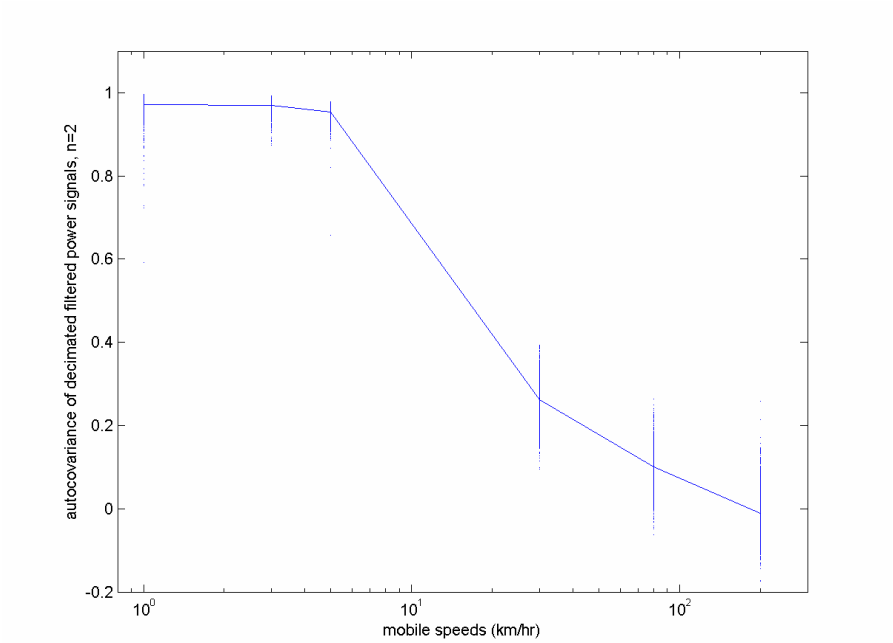

Figure 6-2 *$Cov_D(2)/Cov_D(0) = Cov_D(9.23\ ms)/Cov_D(0\ ms)$* for six speeds with flat Rayleigh channel of 900 MHz radio. (each speed shown 1000 samples dots)

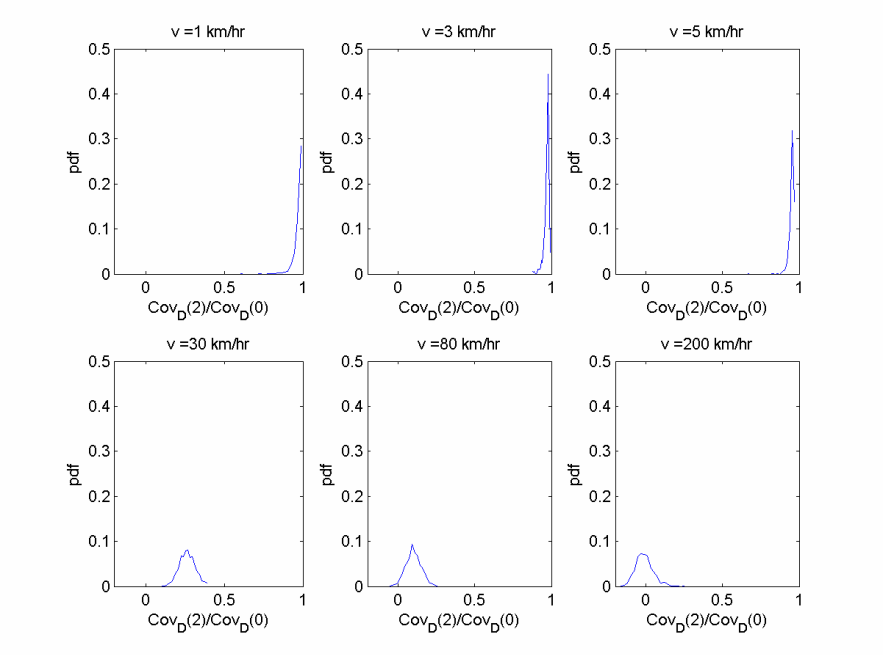

Figure 6-3 Probability density function for the six speeds with flat Rayleigh channel of 900 MHz radio. (based on 1000 samples for each speed)

Actual speed (km/hr)	Estimated speed		
	slow	indeterminate	fast
1	99.9%	0.1%	0%
3	100%	0%	0%
5	100%	0%	0%
30	0%	0%	100%
80	0%	0%	100%
200	0%	0%	100%
≤ 5	**99.97%**	**0.03%**	**0%**
≥ 30	**0%**	**0%**	**100%**

Table 6-1 Mobile speed estimation accuracy for 900 MHz EDGE system with flat Rayleigh fading channel. (based on 1000 samples for each speed)

Actual speed (km/hr)	Estimated speed		
	slow	indeterminate	fast
1	99.8%	0.1%	0.1%
3	100%	0%	0%
5	100%	0%	0%
30	0%	0%	100%
80	0%	0%	100%
200	0%	0%	100%
≤ 5	**99.93%**	**0.03%**	**0.03%**
≥ 30	**0%**	**0%**	**100%**

Table 6-2 Mobile speed estimation accuracy for 900 MHz EDGE system with TU Rayleigh fading channel. (based on 1000 samples for each speed)

Actual speed (km/hr)	Estimated speed		
	slow	indeterminate	fast
1	100%	0%	0%
3	100%	0%	0%
5	100%	0%	0%
30	0%	0%	100%
80	0%	0%	100%
200	0%	0%	100%
≤ 5	**100%**	**0%**	**0%**
≥ 30	**0%**	**0%**	**100%**

Table 6-3 Mobile speed estimation accuracy for 900 MHz EDGE system with HT Rayleigh fading channel. (based on 1000 samples for each speed)

Table 6-1 summarizes the estimation accuracy at 900 MHz EDGE radios with flat Rayleigh fading channel. We also investigate the frequency selective fading channels at typical urban (TU) and hilly terrain (HT) **[12]** profiles, and list their estimation accuracy

Actual speed (km/hr)	Estimated speed		
	slow	indeterminate	fast
1	100%	0%	0%
3	100%	0%	0%
5	100%	0%	0%
30	0%	0%	100%
80	0%	0%	100%
200	0%	0%	100%
≤ 5	**100%**	**0%**	**0%**
≥ 30	**0%**	**0%**	**100%**

Table 6-4 Mobile speed estimation accuracy for 1900 MHz EDGE system with flat Rayleigh fading channel. (based on 1000 samples for each speed)

Actual speed (km/hr)	Estimated speed		
	slow	indeterminate	fast
1	100%	0%	0%
3	100%	0%	0%
5	100%	0%	0%
30	0%	0%	100%
80	0%	0%	100%
200	0%	0%	100%
≤ 5	**100%**	**0%**	**0%**
≥ 30	**0%**	**0%**	**100%**

Table 6-5 Mobile speed estimation accuracy for 1900 MHz EDGE system with TU Rayleigh fading channel. (based on 1000 samples for each speed)

in Table 6-2 and Table 6-3 for 900 MHz systems. Table 6-4 to Table 6-6 show the estimation accuracy at 1900 MHz EDGE systems with flat, TU and HT Rayleigh profiles, respectively.

Actual speed (km/hr)	Estimated speed		
	slow	indeterminate	fast
1	100%	0%	0%
3	100%	0%	0%
5	100%	0%	0%
30	0%	0%	100%
80	0%	0%	100%
200	0%	0%	100%
≤ 5	**100%**	**0%**	**0%**
≥ 30	**0%**	**0%**	**100%**

Table 6-6 Mobile speed estimation accuracy for 1900 MHz EDGE system with HT Rayleigh fading channel. (based on 1000 samples for each speed)

It can be concluded from these tables that our EDGE speed estimation algorithm is very accurate for Rayleigh fading channels, in both flat and frequency selective conditions, for both 900 MHz and 1900 MHz radio systems.

6.3 Simulation Results of Rician Fading Channel

Now we'll verify our speed estimation algorithm for Rician fading channels. Figure 6-4 shows the calculated results of original power signals, filtered power signals, and decimated power signals in 1900 MHz radio with TU Rician fading channel, at mobile speed of 1, 3, 5, 30, 80 and 200 km/hr. In the figure, there is a gap between fast ($v \geq 30$ km/hr) and slow ($v \leq 5$ km/hr) mobiles, and the decimated filtered power signal's autocovariance gives good performance (wide gap) and moderated computation, as the figure of flat Rayleigh fading channel shown in previous section. Since the system is operated at 1900 MHz, we'll examine the autocovariance values at t = 4.615 ms, i.e. one frame delay, according to our algorithm. The figure shows the gap at this moment is wide enough to distinguish the high-speed and low-speed mobiles from their autocovariance

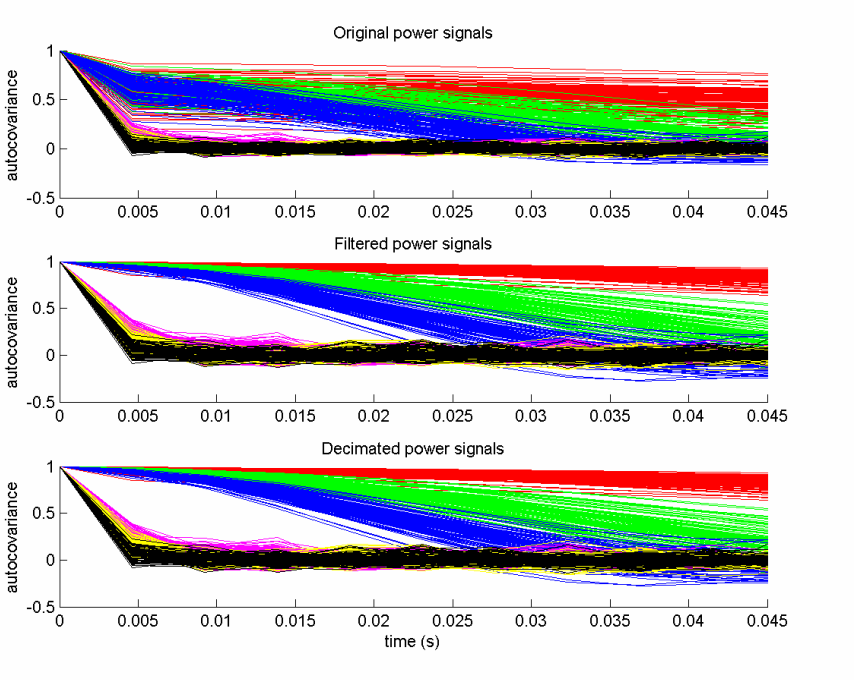

Figure 6-4 Autocovariance of 1900 MHz EDGE system in TU Rician fading channel, mobile speed = 1, 3, 5, 30, 80 and 200 km/hr. (each speed shown 100 sample lines)

values of the decimated filtered power signal.

Now we take the normalized autocovariance value at $n = 1$ ($t = 4.615$ ms) and plot them into six sample speeds as shown in Figure 6-5, where solid lines stand for mean values, and then plot the probability density function of the decimated filtered power signal's autocovariance values in Figure 6-6. From these figures, it can be seen that the thresholds $T_L = 0.65$ and $T_H = 0.55$ we choose in our algorithm are capable of classifying slow- and fast-moving mobiles for Rician fading channels, too.

Table 6-7 to Table 6-9 show the estimation accuracy at 1900 MHz EDGE systems with flat, TU and HT Rician profiles, respectively. And the estimation accuracy at 900 MHz EDGE systems of flat, TU and HT Rician profiles are listed in Table 6-10 to Table 6-12.

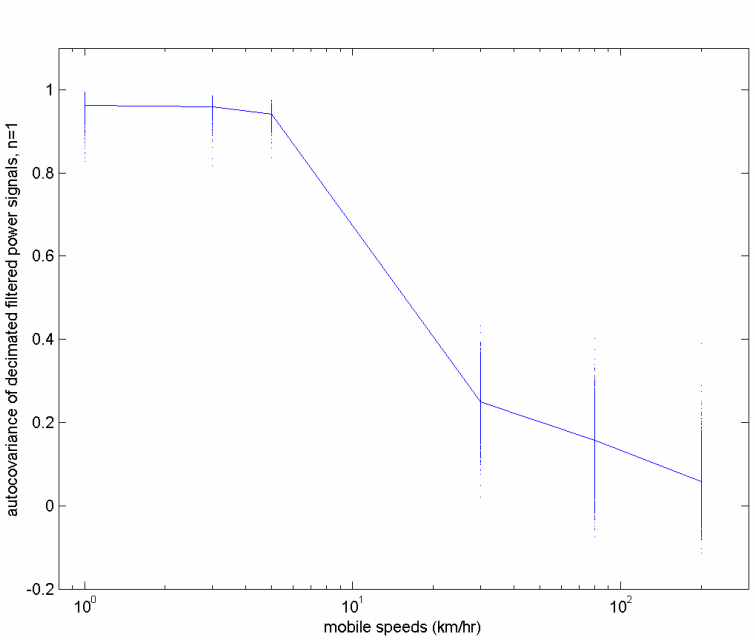

Figure 6-5 $Cov_D(1)/Cov_D(0) = Cov_D(4.615\text{ ms})/Cov_D(0\text{ ms})$ for six speeds with TU Rician channel of 1900 MHz radio. (each speed shown 1000 samples dots)

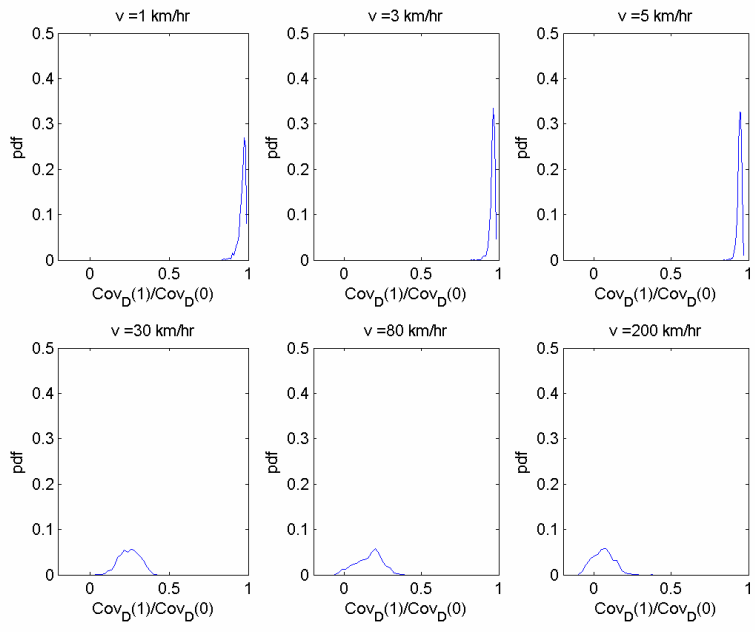

Figure 6-6 Probability density function for the six speeds with TU Rician channel of 1900 MHz radio. (based on 1000 samples for each speed)

Actual speed (km/hr)	Estimated speed		
	slow	indeterminate	fast
1	100%	0%	0%
3	100%	0%	0%
5	100%	0%	0%
30	0%	0%	100%
80	0%	0%	100%
200	0%	0%	100%
≤ 5	**100%**	**0%**	**0%**
≥ 30	**0%**	**0%**	**100%**

Table 6-7 Mobile speed estimation accuracy for 1900 MHz EDGE system with flat Rician fading channel. (based on 1000 samples for each speed)

Actual speed (km/hr)	Estimated speed		
	slow	indeterminate	fast
1	100%	0%	0%
3	100%	0%	0%
5	100%	0%	0%
30	0%	0%	100%
80	0%	0%	100%
200	0%	0%	100%
≤ 5	**100%**	**0%**	**0%**
≥ 30	**0%**	**0%**	**100%**

Table 6-8 Mobile speed estimation accuracy for 1900 MHz EDGE system with TU Rician fading channel. (based on 1000 samples for each speed)

Actual speed (km/hr)	Estimated speed		
	slow	indeterminate	fast
1	100%	0%	0%
3	100%	0%	0%
5	100%	0%	0%
30	0%	0%	100%
80	0%	0%	100%
200	0%	0%	100%
≤ 5	**100%**	**0%**	**0%**
≥ 30	**0%**	**0%**	**100%**

Table 6-9 Mobile speed estimation accuracy for 1900 MHz EDGE system with HT Rician fading channel. (based on 1000 samples for each speed)

Actual speed (km/hr)	Estimated speed		
	slow	indeterminate	fast
1	99.7%	0.1%	0.2%
3	100%	0%	0%
5	100%	0%	0%
30	0%	0%	100%
80	0%	0%	100%
200	0%	0%	100%
≤ 5	**99.9%**	**0.03%**	**0.07%**
≥ 30	**0%**	**0%**	**100%**

Table 6-10 Mobile speed estimation accuracy for 900 MHz EDGE system with flat Rician fading channel. (based on 1000 samples for each speed)

Actual speed (km/hr)	Estimated speed		
	slow	indeterminate	fast
1	100%	0%	0%
3	100%	0%	0%
5	100%	0%	0%
30	0%	0%	100%
80	0%	0%	100%
200	0%	0%	100%
≤ 5	**100%**	**0%**	**0%**
≥ 30	**0%**	**0%**	**100%**

Table 6-11 Mobile speed estimation accuracy for 900 MHz EDGE system with TU Rician fading channel. (based on 1000 samples for each speed)

Actual speed (km/hr)	Estimated speed		
	slow	indeterminate	fast
1	100%	0%	0%
3	100%	0%	0%
5	100%	0%	0%
30	0%	0%	100%
80	0%	0%	100%
200	0%	0%	100%
≤ 5	**100%**	**0%**	**0%**
≥ 30	**0%**	**0%**	**100%**

Table 6-12 Mobile speed estimation accuracy for 900 MHz EDGE system with HT Rician fading channel. (based on 1000 samples for each speed)

It can be concluded from these tables that our EDGE speed estimation algorithm is also very accurate for Rician fading channels, in both flat and frequency selective conditions, for both 900 MHz and 1900 MHz radio systems.

6.4 Remarks and Discussions

The transmitted signal strength is measured by SNR and CIR, and both of them are set to 15 dB in our simulation. If we increase SNR and CIR, which means the transmitted signal is enhanced and the noises and interferences are suppressed, our algorithm will give better estimation results. When SNR and CIR are decreased, more noises and interferences will present in the received signal, and the estimation accuracy of our algorithm will be degraded.

As discussed in Chapter 4, we use 500 slots in our algorithm. If we use fewer slots, sometimes the fading changes very little when the mobiles move very slowly and the fading signal will be totally subtracted as the mean value in autocovariance calculation. From our above simulation results, we see most estimation errors occur at very low speed (v = 1 km/hr) mobiles, because the number of slots is not large enough to provide the sufficient statistics required by the speed estimation algorithm. Therefore, if we increase the slot number N, our method will give better estimation accuracy. The estimator will start to report mobile estimation results about N * 4.615 ms after the communication is established.

Apparently the estimation accuracy of our algorithm is directly related to the speed estimation thresholds. The thresholds $T_L = 0.65$ and $T_H = 0.55$ chosen in this paper are for illustration purpose only, they can be set to other values to get better estimation accuracy in favor of high-speed estimation or low-speed estimation or a compromise for both.

6.5 Conclusion

This chapter presents the simulation result of our mobile speed estimation algorithm of EDGE systems. The simulation results show that our new method is very reliable and effective for estimating mobile speeds in EDGE cellular systems, and it can be used for both Rayleigh and Rician fading channels, flat and frequency selective fading channels, in 900 MHz radios and 1900 MHz radios.

CHAPTER 7

CONCLUSIONS

This thesis was focused on the design, development, analysis, and evaluation of a mobile speed estimation algorithm for practical wireless information system. The algorithm was developed by utilizing the relationship among mobile speed, maximum Doppler spread, and the autocovariance function of the squared envelope (power) of the received signals. By investigating the mathematical model of various wireless propagation environments, we analyzed the statistical properties of different fading environment. The analytical statistical results were then employed to facilitate the design of the new mobile speed estimation algorithm. The algorithm was developed based on the autocovariance function of the received signal power, and it can be applied to a wide range of wireless communication systems with various system configurations. Specifically, the algorithm was tailored according to the system structure of EDGE system, and slot autocovariance function was introduced to avoid the slot burst frequency of EDGE system, which might affect the estimation accuracy. Moreover, an FIR filter was introduced for interference and noise suppression, thus to enhance the estimation accuracy of the proposed mobile speed estimation algorithm.

The mobile speed estimation algorithm was applied to a baseband EDGE system simulator to demonstrate its performance under practical system configurations. Simulation results show that the proposed algorithm can efficiently and accurately discriminate between high-speed mobile users and low-speed mobile users for diverse

wireless propagation environments. For most system configurations, the estimation accuracy is 100%, which means the receiver can completely discriminate low-speed users from high-speed users. The estimation accuracy in the worst-case scenario (v = 1km/hr in 900MHz system) is still as high as 99.7%.

In conclusion, both computer simulation and theoretical analysis showed that the proposed mobile speed estimation algorithm is reliable, efficient, and it can be employed in a wide range of wireless communication system with diverse wireless environments. This mobile speed estimation algorithm can accurately classify the mobile users as fast users and slow users based on their respective speed, and this information could be used by base station or MSC for cell assignment in hierarchical cellular system to avoid frequent handoff, thus to improve the overall system performance.

REFERENCES

[1] L. Wang, M. Silventoinen and Z. Honkasalo, "A new algorithm for estimating mobile speed at the TDMA-based cellular system," in *Proc IEEE Veh. Tech. Conf. VTC'96*, pp. 1145-1149, 1996.

[2] A. Sampath and J. M. Holtzman, "Estimation of maximum Doppler frequency for handoff decisions," in *Proc IEEE Veh. Tech. Conf. VTC'93*, pp. 859-862, 1993.

[3] C. Tepedelenlioglu and G. B. Giannakis, "On velocity estimation and correlation properties of narrow-band mobile communication channels," *IEEE Trans. Veh. Technol.*, vol. 50, pp. 1039-1052, Jul. 2001.

[4] C. Xiao, K. D. Mann and J. C. Olivier, "Mobile Speed Estimation for TDMA-Based Hierarchical Cellular Systems," *IEEE Trans. Veh. Technol.*, vol. 50, pp. 981-991, Jul. 2001.

[5] C. Xiao, "Estimating Velocity of Mobiles in EDGE Systems," in *Proc IEEE Intern. Conf. Commun. ICC 02*, vol. 5, pp. 3240-3244, May 2002.

[6] J.D. Parson, *The mobile radio propagation channel*, 2nd ed. John Wiley & Sons, 2000.

[7] A. Papoulis, S.U. Pillai, *Probability, random variables and stochastic processes*, 4th ed. New York, NY: McGraw-Hill, 2002.

[8] M.K. Simon, and M.-S. Alouini, *Digital communication over fading channels: a unified approach to performance analysis*, New York:John Wiley & Sons, 2000..

[9] K. Feher, *Wireless Digital Communications—Modulation & Spread Spectrum Applications*. Englewood Cliffs, NJ: Prentice-Hall, 1995.

[10] P. P. Vaidyanathan, *Multirate Systems and Filter Banks*. Englewood Cliffs, NJ: Prentice-Hall, 1993.

[11] R. Zheng and C. Xiao, "Statistical Simulation Models for Rayleigh and Rician Fading," in *Proc Intern. Conf. Commun. ICC 03*, vol. 5, pp. 3524-3529, May 2003.

[12] ETSI. GSM 05.05, "Radio transmission and reception," ETSI EN 300 910 V8.5.1, Nov. 2000.

APPENDIX

DERIVATION OF EQUATIONS

A.1 Derivation of Equation (2.17)

Using (2.13), we have $g_I(t) = \sum_{n=1}^{N} \alpha_n \cos\phi_n(t)$, then

$$R_{g_I g_I}(\tau) = \mathrm{E}[g_I(t) g_I(t+\tau)]$$

$$= \mathrm{E}\{[\sum_{n=1}^{N} \alpha_n \cos\phi_n(t)][\sum_{m=1}^{N} \alpha_m \cos\phi_m(t+\tau)]\}$$

$$= \mathrm{E}[\sum_{n=1}^{N}\sum_{m=1}^{N} \alpha_n \alpha_m \cos\phi_n(t)\cos\phi_m(t+\tau)]$$

$$= \mathrm{E}\{\sum_{n=1}^{N}\sum_{m=1}^{N} \alpha_n \alpha_m \frac{\cos[\phi_n(t)+\phi_m(t+\tau)] + \cos[\phi_n(t)-\phi_m(t+\tau)]}{2}\}$$

From (2.9), we know

$$\phi_n(t) = -2\pi\{(f_c + f_D)\tau_n - f_D t\} \text{ and } \phi_m(t+\tau) = -2\pi\{(f_c + f_D)\tau_m - f_D(t+\tau)\}.$$

Since f_c is very large, and τ_n, τ_m are random variables, the phases $\phi_n(t)$ and $\phi_m(t+\tau)$ can be assumed to be uniformly distributed over $[-\pi, \pi]$. Furthermore, the phases $\phi_n(t)$ and $\phi_m(t+\tau)$ are independent because their associated propagation paths are independent for $m \neq n$. So the expectation equals to 0 if $m \neq n$. Thus

$$R_{g_I g_I}(\tau) = \mathrm{E}[\sum_{n=1}^{N} \alpha_n^2 \frac{\cos(\phi_n(t)+\phi_n(t+\tau)) + \cos(\phi_n(t)-\phi_n(t+\tau))}{2}].$$

Since α_n and $\phi_n(t)$ are independent,

$$R_{g_I g_I}(\tau) = \sum_{n=1}^{N} \mathrm{E}[\frac{\alpha_n^2}{2}]\mathrm{E}[\cos(\phi_n(t) + \phi_n(t+\tau)) + \cos(\phi_n(t) - \phi_n(t+\tau))]$$

$$= \sum_{n=1}^{N} \mathrm{E}[\frac{\alpha_n^2}{2}]\mathrm{E}[\cos(2\pi f_D \tau)].$$

Define the total signal power $\Omega_p = \sum_{n=1}^{N} \mathrm{E}[\alpha_n^2]$,

$$R_{g_I g_I}(\tau) = \frac{\Omega_p}{2} \mathrm{E}[\cos(2\pi f_D \tau)].$$

Substitute f_D according to (2.1),

$$R_{g_I g_I}(\tau) = \frac{\Omega_p}{2} \mathrm{E}[\cos(2\pi f_M \tau \cos\theta)]. \qquad \text{(A.1)}$$

In Rayleigh fading channel, it is reasonable to assume that the multi-path waves arrive at mobile station from all directions with same probability, so θ is uniformly distributed over $[-\pi, \pi]$. Then

$$R_{g_I g_I}(\tau) = \frac{\Omega_p}{2} \frac{1}{2\pi} \int_{-\pi}^{\pi} \cos(2\pi f_M \tau \cos\theta) d\theta$$

$$= \frac{\Omega_p}{2} \frac{1}{\pi} \int_{0}^{\pi} \cos(2\pi f_M \tau \cos\theta) d\theta$$

$$= \frac{\Omega_p}{2} J_0(2\pi f_M \tau).$$

With similar procedures, we can prove equation (2.18) by

$$R_{g_Q g_Q}(\tau) = \frac{\Omega_p}{2} J_0(2\pi f_M \tau) = R_{g_I g_I}(\tau).$$

A.2 Derivation of Equation (2.19)

Based on (2.13) and (2.14) and the results in the previous section,

$$
\begin{aligned}
R_{g_I g_Q}(\tau) &= \mathrm{E}[g_I(t) g_Q(t+\tau)] \\
&= \mathrm{E}[\sum_{n=1}^{N} \alpha_n \cos\phi_n(t) \sum_{m=1}^{N} \alpha_m \sin\phi_m(t+\tau)] \\
&= \mathrm{E}\{\sum_{n=1}^{N}\sum_{m=1}^{N} \alpha_n \alpha_m \frac{\sin[\phi_m(t+\tau)+\phi_n(t)] + \sin[\phi_m(t+\tau)-\phi_n(t)]}{2}\} \\
&= \mathrm{E}[\sum_{n=1}^{N} \alpha_n^2 \frac{\sin(\phi_n(t+\tau)+\phi_n(t)) + \sin(\phi_n(t+\tau)-\phi_n(t))}{2}] \\
&= \sum_{n=1}^{N} \mathrm{E}[\frac{\alpha_n^2}{2}]\mathrm{E}[\sin(2\pi f_D \tau)] \\
&= \frac{\Omega_p}{2}\mathrm{E}[\sin(2\pi f_M \tau \cos\theta)] \qquad \text{(A.2)} \\
&= \frac{\Omega_p}{2}\frac{1}{2\pi}\int_{-\pi}^{\pi} \sin(2\pi f_M \tau \cos\theta) d\theta \\
&= 0
\end{aligned}
$$

Following the same procedure, equation (2.20) can be proved.

A.3 Derivation of Equation (2.21)

By using (2.12), $R_{gg}(\tau)$ can be derived as

$$
\begin{aligned}
R_{gg}(\tau) &= \frac{1}{2}\mathrm{E}[g^*(t) g(t+\tau)] \\
&= \frac{1}{2}\mathrm{E}\{[(g_I(t) - jg_Q(t)][g_I(t+\tau) + jg_Q(t+\tau)]\} \\
&= \frac{1}{2}\mathrm{E}[g_I(t)g_I(t+\tau) + jg_I(t)g_Q(t+\tau) - jg_Q(t)g_I(t+\tau) + g_Q(t)g_Q(t+\tau)] \\
&= \frac{1}{2}[R_{g_I g_I}(\tau) + jR_{g_I g_Q}(\tau) - jR_{g_Q g_I}(\tau) + R_{g_Q g_Q}(\tau)]
\end{aligned}
$$

From (2.18) and (2.20), we'll get

$$
R_{gg}(\tau) = R_{g_I g_I}(\tau) + jR_{g_I g_Q}(\tau) .
$$

This completes the proof.

A.4 Derivation of Equation (2.22)

Since $g(t) = g_I(t) + jg_Q(t)$, so $|g(t)|^2 = g_I^2(t) + g_Q^2(t)$, then

$$R_{|g|^2|g|^2}(\tau) = \mathrm{E}[|g(t)|^2 |g(t+\tau)|^2]$$

$$= \mathrm{E}\{[g_I^2(t) + g_Q^2(t)][g_I^2(t+\tau) + g_Q^2(t+\tau)]\}$$

$$= \mathrm{E}[g_I^2(t)g_I^2(t+\tau) + g_I^2(t)g_Q^2(t+\tau) + g_Q^2(t)g_I^2(t+\tau) + g_Q^2(t)g_Q^2(t+\tau)] \quad \text{(A.3)}$$

In flat fading channel, both of the quadrature components $g_I(t)$ and $g_Q(t)$ are zero-mean Gaussian distributed. If x_1, x_2, x_3 and x_4 are zero-mean Gaussian random variables, then $\mathrm{E}[x_1x_2x_3x_4] = \mathrm{E}[x_1x_2]\mathrm{E}[x_3x_4] + \mathrm{E}[x_1x_3]\mathrm{E}[x_2x_4] + \mathrm{E}[x_1x_4]\mathrm{E}[x_2x_3]$.

Hence

$$\mathrm{E}[g_I^2(t)g_I^2(t+\tau)] = \mathrm{E}[g_I(t)g_I(t)]\mathrm{E}[g_I(t+\tau)g_I(t+\tau)] + 2\mathrm{E}[g_I(t)g_I(t+\tau)]\mathrm{E}[g_I(t)g_I(t+\tau)]$$
$$= R_{g_Ig_I}^2(0) + 2R_{g_Ig_I}^2(\tau), \quad \text{(A.4)}$$

$$\mathrm{E}[g_I^2(t)g_Q^2(t+\tau)] = \mathrm{E}[g_I(t)g_I(t)]\mathrm{E}[g_Q(t+\tau)g_Q(t+\tau)] + 2\mathrm{E}[g_I(t)g_Q(t+\tau)]\mathrm{E}[g_I(t)g_Q(t+\tau)]$$
$$= R_{g_Ig_I}(0)R_{g_Qg_Q}(0) + 2R_{g_Ig_Q}^2(\tau),$$

$$\mathrm{E}[g_Q^2(t)g_I^2(t+\tau)] = R_{g_Qg_Q}(0)R_{g_Ig_I}(0) + 2R_{g_Qg_I}^2(\tau),$$

and

$$\mathrm{E}[g_Q^2(t)g_Q^2(t+\tau)] = R_{g_Qg_Q}^2(0) + 2R_{g_Qg_Q}^2(\tau).$$

Therefore

$$R_{|g|^2|g|^2}(\tau) = [R_{g_Ig_I}^2(0) + 2R_{g_Ig_I}^2(\tau)] + [R_{g_Ig_I}(0)R_{g_Qg_Q}(0) + 2R_{g_Ig_Q}^2(\tau)] +$$

$$[R_{g_Qg_Q}(0)R_{g_Ig_I}(0) + 2R_{g_Qg_I}^2(\tau)] + [R_{g_Qg_Q}^2(0) + 2R_{g_Qg_Q}^2(\tau)].$$

Since $R_{g_Qg_Q}(\tau) = R_{g_Ig_I}(\tau)$ and $R_{g_Qg_I}(\tau) = -R_{g_Ig_Q}(\tau)$,

$$R_{|g|^2|g|^2}(\tau) = 4R_{g_Ig_I}^2(0) + 4R_{g_Ig_I}^2(\tau) + 4R_{g_Ig_Q}^2(\tau).$$

The proof of (2.22) is completed.

A.5 Derivation of Equation (2.23)

The autocovariance of the power of fading signal is

$$\Phi_{|g|^2|g|^2}(\tau) = \mathrm{E}\{|g(t)|^2 - \mathrm{E}[|g(t)|^2]\}$$

$$\begin{aligned}
&= \mathrm{E}[(|g(t)|^2 - \mathrm{E}[|g(t)|^2])(|g(t+\tau)|^2 - \mathrm{E}[|g(t+\tau)|^2])] \\
&= \mathrm{E}\{|g(t)|^2 |g(t+\tau)|^2 - |g(t)|^2 \mathrm{E}[|g(t+\tau)|^2] - \mathrm{E}[|g(t)|^2]|g(t+\tau)|^2 + \mathrm{E}[|g(t)|^2]\mathrm{E}[|g(t+\tau)|^2]\} \\
&= R_{|g|^2|g|^2}(\tau) - \mathrm{E}[|g(t)|^2]\mathrm{E}[|g(t+\tau)|^2] - \mathrm{E}[|g(t)|^2]\mathrm{E}[|g(t+\tau)|^2] + \mathrm{E}[|g(t)|^2]\mathrm{E}[|g(t+\tau)|^2] \\
&= R_{|g|^2|g|^2}(\tau) - \mathrm{E}[|g(t)|^2]\mathrm{E}[|g(t+\tau)|^2] \\
&= R_{|g|^2|g|^2}(\tau) - \mathrm{E}^2[|g(t)|^2] \\
&= R_{|g|^2|g|^2}(\tau) - \mathrm{E}^2[g_I^2(t) + g_Q^2(t)] \\
&= R_{|g|^2|g|^2}(\tau) - (\mathrm{E}[g_I^2(t)] + \mathrm{E}[g_Q^2(t)])^2 \\
&= R_{|g|^2|g|^2}(\tau) - [R_{g_I g_I}(0) + R_{g_Q g_Q}(0)]^2 \\
&= R_{|g|^2|g|^2}(\tau) - 4R_{g_I g_I}^2(0) \\
&= 4R_{g_I g_I}^2(\tau) + 4R_{g_I g_Q}^2(\tau).
\end{aligned} \tag{A.5}$$

A.6 Derivation of Equation (2.25)

In section A.1, we obtained (A.1) as

$$R_{g_I g_I}(\tau) = \frac{\Omega_p}{2}\mathrm{E}[\cos(2\pi f_M \tau \cos\theta)].$$

For Rician fading channel, the pdf of incident angle θ is

$$p(\theta) = \frac{1}{K+1}\hat{p}(\theta) + \frac{K}{K+1}\delta(\theta - \theta_0) \qquad (-\pi \le \theta \le \pi), \tag{A.6}$$

where K is the Rician factor, θ_0 is the angle of the LOS path, and $\hat{p}(\theta)$ is the pdf of uniform distribution over $[-\pi, \pi]$ and is defined as $\hat{p}(\theta) = \frac{1}{2\pi}$ $(-\pi \le \theta \le \pi)$.

Thus

$$\begin{aligned} R_{g_I g_I}(\tau) &= \frac{\Omega_p}{2}\left[\frac{1}{K+1}\frac{1}{2\pi}\int_{-\pi}^{\pi}\cos(2\pi f_M \tau\cos\theta)d\theta + \frac{K}{K+1}\int_{-\pi}^{\pi}\cos(2\pi f_M \tau\cos\theta)\delta(\theta-\theta_0)d\theta\right] \\ &= \frac{\Omega_p}{2}\left[\frac{1}{K+1}\frac{1}{\pi}\int_{0}^{\pi}\cos(2\pi f_M \tau\cos\theta)d\theta + \frac{K}{K+1}\cos(2\pi f_M \tau\cos\theta_0)\right] \\ &= \frac{1}{K+1}\frac{\Omega_p}{2}J_0(2\pi f_M \tau) + \frac{K}{K+1}\frac{\Omega_p}{2}\cos(2\pi f_M \tau\cos\theta_0). \end{aligned}$$

The proof is completed, and (2.26) can be proved following the same procedure.

A.7 Derivation of Equation (2.27)

During the proof of (2.19) in section A.2, $R_{g_I g_Q}(\tau)$ is simplified to (A.2) as

$$R_{g_I g_Q}(\tau) = \frac{\Omega_p}{2}\mathrm{E}[\sin(2\pi f_M \tau\cos\theta)].$$

Employing the pdf of θ described in section A.6 as (A.6) leads to

$$\begin{aligned} R_{g_I g_Q}(\tau) &= \frac{\Omega_p}{2}\left[\frac{1}{K+1}\frac{1}{2\pi}\int_{-\pi}^{\pi}\sin(2\pi f_M \tau\cos\theta)d\theta + \frac{K}{K+1}\int_{-\pi}^{\pi}\sin(2\pi f_M \tau\cos\theta)\delta(\theta-\theta_0)d\theta\right] \\ &= \frac{\Omega_p}{2}\left[\frac{1}{K+1}0 + \frac{K}{K+1}\sin(2\pi f_M \tau\cos\theta_0)\right] \\ &= \frac{K}{K+1}\frac{\Omega_p}{2}\sin(2\pi f_M \tau\cos\theta_0). \end{aligned}$$

The derivation is completed.

A.8 Derivation of Equation (2.30)

From (A.3), which is proved in section A.4,

$$R_{|g|^2|g|^2}(\tau) = \mathrm{E}[g_I^2(t)g_I^2(t+\tau) + g_I^2(t)g_Q^2(t+\tau) + g_Q^2(t)g_I^2(t+\tau) + g_Q^2(t)g_Q^2(t+\tau)].$$

Suppose

$$g_I(t) = \hat{g}_I(t) + m_I(t), \qquad g_Q(t) = \hat{g}_Q(t) + m_Q(t),$$

where $m_I(t)$ and $m_Q(t)$ are the quadrature components of the LOS path of the Rician fading signal with

$$m_I(t) = \sqrt{\Omega_L}\cos(2\pi f_M \tau \cos\theta_0), \qquad m_Q(t) = \sqrt{\Omega_L}\sin(2\pi f_M \tau \cos\theta_0),$$

where Ω_L is the power of the specular component and is proportional to the total Rician fading signal power as $\Omega_L = \frac{K}{K+1}\Omega_P$.

The functions $\hat{g}_I(t)$, $\hat{g}_Q(t)$ represent the quadrature components of the scattered paths of the Rician fading signal, so $\hat{g}_I(t)$ and $\hat{g}_Q(t)$ are zero-mean Gaussian distributed.

Then the first part of $R_{|g|^2|g|^2}(\tau)$ can be written as

$$\begin{aligned}
&\mathrm{E}[g_I^2(t)g_I^2(t+\tau)] = \\
&\mathrm{E}\{[\hat{g}_I^2(t) + 2m_I(t)\hat{g}_I(t) + m_I^2(t)][\hat{g}_I^2(t+\tau) + 2m_I(t+\tau)\hat{g}_I(t+\tau) + m_I^2(t+\tau)]\} \\
&= \mathrm{E}[\hat{g}_I^2(t)\hat{g}_I^2(t+\tau) + 2m_I(t+\tau)\hat{g}_I^2(t)\hat{g}_I(t+\tau) + m_I^2(t+\tau)\hat{g}_I^2(t) \\
&+2m_I(t)\hat{g}_I(t)\hat{g}_I^2(t+\tau) + 4m_I(t)m_I(t+\tau)\hat{g}_I(t)\hat{g}_I(t+\tau) + 2m_I(t)m_I^2(t+\tau)\hat{g}_I(t) \\
&+m_I^2(t)\hat{g}_I^2(t+\tau) + 2m_I^2(t)m_I(t+\tau)\hat{g}_I(t+\tau) + m_I^2(t)m_I^2(t+\tau)]
\end{aligned} \tag{A.7}$$

If x_1, x_2 and x_3 are zero-mean Gaussian random variables, then

$$\mathrm{E}[x_1x_2x_3] = \mathrm{E}[x_1]\mathrm{E}[x_2x_3] + \mathrm{E}[x_2]\mathrm{E}[x_1x_3] + \mathrm{E}[x_3]\mathrm{E}[x_1x_2] + 2\mathrm{E}[x_1]\mathrm{E}[x_2]\mathrm{E}[x_3].$$

And $\mathrm{E}[\hat{g}_I(t)] = 0$ due to the fact that $\hat{g}_I(t)$ is zero-mean Gaussian distributed. Also from (A.4) in section A.4, we know $\mathrm{E}[\hat{g}_I^2(t)\hat{g}_I^2(t+\tau)] = R^2_{\hat{g}_I\hat{g}_I}(0) + 2R^2_{\hat{g}_I\hat{g}_I}(\tau)$, so

$$\mathrm{E}[g_I^2(t)g_I^2(t+\tau)] = R^2_{\hat{g}_I\hat{g}_I}(0) + 2R^2_{\hat{g}_I\hat{g}_I}(\tau) + m_I^2(t+\tau)R_{\hat{g}_I\hat{g}_I}(0)$$
$$+4m_I(t)m_I(t+\tau)R_{\hat{g}_I\hat{g}_I}(\tau) + m_I^2(t)R_{\hat{g}_I\hat{g}_I}(0) + m_I^2(t)m_I^2(t+\tau)$$

With the same rules and $R_{\hat{g}_Q\hat{g}_Q}(\tau) = R_{\hat{g}_I\hat{g}_I}(\tau)$, the fourth part $\mathrm{E}[g_Q^2(t)g_Q^2(t+\tau)]$ of (A.7) can be written as

$$\mathrm{E}[g_Q^2(t)g_Q^2(t+\tau)] = R^2_{\hat{g}_I\hat{g}_I}(0) + 2R^2_{\hat{g}_I\hat{g}_I}(\tau) + m_Q^2(t+\tau)R_{\hat{g}_I\hat{g}_I}(0)$$
$$+4m_Q(t)m_Q(t+\tau)R_{\hat{g}_I\hat{g}_I}(\tau) + m_Q^2(t)R_{\hat{g}_I\hat{g}_I}(0) + m_Q^2(t)m_Q^2(t+\tau)$$

The second part of (A.7) is

$$\mathrm{E}[g_I^2(t)g_Q^2(t+\tau)] =$$
$$\mathrm{E}\{[\hat{g}_I^2(t) + 2m_I(t)\hat{g}_I(t) + m_I^2(t)][\hat{g}_Q^2(t+\tau) + 2m_Q(t+\tau)\hat{g}_Q(t+\tau) + m_Q^2(t+\tau)]\}$$
$$= \mathrm{E}[\hat{g}_I^2(t)\hat{g}_Q^2(t+\tau) + 2m_Q(t+\tau)\hat{g}_I^2(t)\hat{g}_Q(t+\tau) + m_Q^2(t+\tau)\hat{g}_I^2(t)$$
$$+2m_I(t)\hat{g}_I(t)\hat{g}_Q^2(t+\tau) + 4m_I(t)m_Q(t+\tau)\hat{g}_I(t)\hat{g}_Q(t+\tau) + 2m_I(t)m_Q^2(t+\tau)\hat{g}_I(t)$$
$$+m_I^2(t)\hat{g}_Q^2(t+\tau) + 2m_I^2(t)m_Q(t+\tau)\hat{g}_Q(t+\tau) + m_I^2(t)m_Q^2(t+\tau)]$$

Since $\mathrm{E}[\hat{g}_I^2(t)\hat{g}_Q^2(t+\tau)] = = R_{\hat{g}_I\hat{g}_I}(0)R_{\hat{g}_Q\hat{g}_Q}(0) + 2R^2_{\hat{g}_I\hat{g}_Q}(\tau)$, $R_{\hat{g}_Q\hat{g}_Q}(\tau) = R_{\hat{g}_I\hat{g}_I}(\tau)$, $R_{\hat{g}_I\hat{g}_Q}(\tau) = 0$, and $\mathrm{E}[\hat{g}_I(t)] = 0$,

$$\mathrm{E}[g_I^2(t)g_Q^2(t+\tau)] = R^2_{\hat{g}_I\hat{g}_I}(0) + m_Q^2(t+\tau)R_{\hat{g}_I\hat{g}_I}(0) + m_I^2(t)R_{\hat{g}_I\hat{g}_I}(0) + m_I^2(t)m_Q^2(t+\tau).$$

With the same rules and $R_{\hat{g}_Q\hat{g}_I}(\tau) = 0$, the third part of (A.7), $\mathrm{E}[g_Q^2(t)g_I^2(t+\tau)]$, can be written as

$$\mathrm{E}[g_Q^2(t)g_I^2(t+\tau)] = R^2_{\hat{g}_I\hat{g}_I}(0) + m_I^2(t+\tau)R_{\hat{g}_I\hat{g}_I}(0) + m_Q^2(t)R_{\hat{g}_I\hat{g}_I}(0) + m_Q^2(t)m_I^2(t+\tau).$$

Combining above four parts together, we have

$$R_{|g|^2|g|^2}(\tau) = 4R^2_{\hat{g}_I \hat{g}_I}(0) + 4R^2_{\hat{g}_I \hat{g}_I}(\tau) + 2[m_I^2(t+\tau) + m_Q^2(t+\tau)]R_{\hat{g}_I \hat{g}_I}(0)$$
$$+4[m_I(t)m_I(t+\tau) + m_Q(t)m_Q(t+\tau)]R_{\hat{g}_I \hat{g}_I}(\tau) + 2[m_I^2(t) + m_Q^2(t)]R_{\hat{g}_I \hat{g}_I}(0).$$
$$+[m_I^2(t) + m_Q^2(t)][m_I^2(t+\tau) + m_Q^2(t+\tau)]$$

Since $R_{\hat{g}_I \hat{g}_I}(\tau) = \frac{\Omega_R}{2} J_0(2\pi f_M \tau)$ where $\Omega_R = \frac{1}{K+1}\Omega_P$ is the power of all scattered components and $m_I^2(t) + m_Q^2(t) = \Omega_L = \frac{K}{K+1}\Omega_P$, and

$$m_I(t)m_I(t+\tau) = \Omega_L \cos(2\pi f_M \tau \cos\theta_0)\cos(2\pi f_M (t+\tau)\cos\theta_0)$$
$$= \frac{\Omega_L}{2}[\cos(2\pi f_M (2t+\tau)\cos\theta_0) + \cos(2\pi f_M \tau \cos\theta_0)] \quad ,$$

$$m_Q(t)m_Q(t+\tau) = \Omega_L \sin(2\pi f_M \tau \cos\theta_0)\sin(2\pi f_M (t+\tau)\cos\theta_0)$$
$$= \frac{\Omega_L}{2}[\cos(2\pi f_M \tau \cos\theta_0) - \cos(2\pi f_M (2t+\tau)\cos\theta_0)] \quad ,$$

So

$$R_{|g|^2|g|^2}(\tau) = \Omega_R^2 + \Omega_R^2 J_0^2(2\pi f_M \tau) + 2\Omega_L\Omega_R + 2\Omega_L\Omega_R \cos(2\pi f_M \tau \cos\theta_0) J_0(2\pi f_M \tau) + \Omega_L^2$$

$$= (\frac{\Omega_P}{K+1})^2 (1 + 2K + K^2 + J_0^2(2\pi f_M \tau) + 2KJ_0(2\pi f_M \tau)\cos(2\pi f_M \tau \cos\theta_0)).$$

A.9 Derivation of Equation (2.31)

With (A.5) derived in section A.5

$$\Phi_{|g|^2|g|^2}(\tau) = R_{|g|^2|g|^2}(\tau) - \mathrm{E}^2[|g(t)|^2],$$

where $\mathrm{E}[|g(t)|^2] = \mathrm{E}[g_I^2(t) + g_Q^2(t)]$

$$= \mathrm{E}[\hat{g}_I^2(t) + 2m_I(t)\hat{g}_I(t) + m_I^2(t) + \hat{g}_Q^2(t) + 2m_Q(t)\hat{g}_Q(t) + m_Q^2(t)]$$
$$= 2R_{\hat{g}_I \hat{g}_I}(0) + \Omega_L$$

We have

$$\Phi_{|g|^2|g|^2}(\tau) = R_{|g|^2|g|^2}(\tau) - (2R_{\hat{g}_I \hat{g}_I}(0) + \Omega_L)^2$$

$$= R_{|g|^2|g|^2}(\tau) - (\Omega_R + \Omega_L)^2$$

$$= R_{|g|^2|g|^2}(\tau) - (\frac{1}{K+1}\Omega_p + \frac{K}{K+1}\Omega_p)^2$$

$$= R_{|g|^2|g|^2}(\tau) - (\frac{\Omega_p}{K+1})^2(1+K)^2$$

$$= (\frac{\Omega_P}{K+1})^2(J_0^2(2\pi f_M \tau) + 2KJ_0(2\pi f_M \tau)\cos(2\pi f_M \tau \cos\theta_0))$$

This completes the derivation.